Human-induced climate change compounded by socio-economic water stressors increased severity of drought in Syria, Iraq and Iran

Authors

Friederike E. L Otto, *Grantham Institute, Imperial College London, UK*
Ben Clarke, *Grantham Institute, Imperial College, London, UK*
Mohammad Rahimi, *Faculty of Desert Studies, Semnan University, Semnan, Iran*
Mariam Zachariah, *Grantham Institute, Imperial College, London, UK*
Clair Barnes, *Grantham Institute, Imperial College London, UK*
Joyce Kimutai, *Grantham Institute, Imperial College London, UK*
Simphiwe Stewart, *Red Cross Red Crescent Climate Centre, The Hague, the Netherlands*
Maja Vahlberg, *Red Cross Red Crescent Climate Centre, The Hague, the Netherlands*
Abhinav Banthiya, *Red Cross Red Crescent Climate Centre, The Hague, the Netherlands*
Rana El Hajj, *Red Cross Red Crescent Climate Centre, The Hague, the Netherlands*

Review authors

Roop Singh, *Red Cross Red Crescent Climate Centre, The Hague, the Netherlands*
Alex Wynter, *Red Cross Red Crescent Climate Centre, The Hague, the Netherlands*
Sjoukje Philip, *Royal Netherlands Meteorological Institute (KNMI), De Bilt, The Netherlands*
Izidine Pinto, *Royal Netherlands Meteorological Institute (KNMI), De Bilt, The Netherlands*

Main findings

- The drought affects a region with a highly vulnerable population due to varying degrees of fragility and conflict including war and post-war transition, rapid urbanisation in the face of limited technical capacity, and regional instability. These dynamics increased vulnerability to the impacts of drought and created a humanitarian crisis.
- The whole Euphrates and Tigris basin (ET-basin) and large parts of Iran experienced extreme and exceptional agricultural drought over the 36 months up to June 2023, making it the second-worst drought on record in both regions based on SPEI.
- The extreme nature of the drought is not rare in the present climate (which has been warmed by 1.2°C due to burning of fossil fuels). Events of comparable severity are expected to occur at least every decade.
- Using three different observations-based data products we find a strong trend towards more severe droughts in both regions. We find that the combination of low rainfall and high evapotranspiration as unusual as the recent conditions - that is, an event that occurred around every 5-10 years - in a world that had not been warmed 1.2°C would be so much less severe that nowadays it would not be classified as a drought at all.
- In order to identify whether and to what extent human-induced climate change was a driver of these trends we combine observations-based data products and climate models and look at the

36-month SPEI in both regions. We find that over the ET-basin the likelihood of such a drought occurring has increased by a factor of 25 compared to a 1.2°C cooler world. Over Iran the likelihood of such a drought occurring has increased by a factor of 16 compared to a 1.2°C cooler world.

- For both regions human-induced climate change has increased the intensity of such a drought such that it would not have been classified as a drought in a 1.2°C cooler world. Thus confirming that the observed finding is indeed caused by human-induced climate change.
- To understand the meteorological drivers behind this change in agricultural drought we also analysed rainfall and temperature separately and found there to be little change in the likelihood and intensity of rainfall but a very large increase in temperature. We thus conclude that this strong increase in drought severity is primarily driven by the very strong increase in extreme temperatures due to the burning of fossil fuels.
- Unless the world rapidly stops burning fossil fuels, these events will become even more common in the future. In a world 2°C warmer than preindustrial an event like this would be an exceptional drought, the worst category possible.
- The high levels of water stress in the region today are exacerbated by limitations in technical capacity, water management, and regional cooperation. Rapid population growth, industrialization and land-use changes, dam practices and river flow management between upstream and downstream countries, aged water treatment plants, and low efficiency of irrigation water systems have contributed to a complex water crisis. Water is moreover weaponised in conflict, with water systems increasingly targeted for sabotage.
- These results highlight that despite 'low confidence' in IPCC projections for drought in the region, increasing water stress driven by human-induced climate change as well as other systemic factors continues to be a major threat for the population and requires urgent efforts for more effective water management strategies, interdisciplinary humanitarian response, and regional cooperation that includes farmers and other stakeholders in the planning.

1 Introduction

From boreal winter 2020 onwards, a large region in West Asia encompassing Iran, Iraq, and Syria suffered from exceptionally low rains that have been reported to be up to 95% below average (Al-Monitor, 2023). The resulting 3-year drought has led to severe impacts on agriculture, in a region where a large part of the population depends on wheat farming and livestock. With Iran being the region's highest wheat producer the country had to rely on imports, leading to soaring prices for basic food items (Gro Intelligence, 2023). In Iran, unprecedented and widespread drought was first recorded in July 2021 where 29 of 31 provinces especially South Khorasan, Kerman, Sistan Balochistan, Hormozgan, Khuzestan, Isfahan, Khorasan Razavi have been severely affected (IFRC, 2023). Households in the country face broad based challenges related to a lack of access to safe and sufficient water supply for drinking, hygiene, agriculture and animal husbandry, and electrical power resulting in negative social trends and coping mechanisms (IFRC, 2022).

Harvests in the three years 2021-2023 have been even more severely affected in Syria, where 11 years of conflict severely limited the coping capacity of the population, leading to 12 million people facing hunger (ICRC, 2023). In Syria, the World Meteorological Organisation (WMO) seasonal outlook indicates severe and long term drought accompanied by water deficits, unusual dry conditions during the wet season, and abnormally high air temperatures which are expected to continue throughout the

hot and dry seasons of July – September this year (ECHO, 2022). The multi-year drought and its compounding impacts on the price(s) of goods and services - including food, water, and energy – as well as outbreaks in Cholera have made access to water one of the most prominent humanitarian challenges across the country. This is especially true for Al-Sweida governorate which has faced a dynamic set of challenges since 2010 including an influx of displaced people, increasing demand on water and pressure on resources, at the same time as maintenance and technical levels of logistical operating equipment have decreased due to governance challenges, illegal extraction, and a rise in vandalism among other socio-economic issues (IFRC, 2023).

In Iraq, where agriculture is the principal source of income and livelihoods, the interlinked drought and climate crisis is even more complex. The intersecting impacts of climate change, economic and fiscal policy, as well as dam practices affecting river flow from neighbouring countries has compounded the impacts of drought and poor water quality with devastating impacts especially for vulnerable populations across the country who are already exposed to conflict-related displacement (Norwegian Refugee Council, 2022). Surveys by the Norwegian Refugee Council suggest widespread crop failure, reductions in net profit, and increased reliance on social assistance which further exacerbates existing socio-economic challenges in the country (ibid, 2022). In addition to agricultural impacts, the drought particularly affected access to drinking water, with 6 out of 10 households facing water shortages and fishermen having to abandon their livelihoods as rivers, wetlands and lakes have dried up (Alarabia, 2023). Between 2016 - 2022, IOM data suggests 55,290 people were displaced by climate and environmental degradation in South and Central Iraq (UNOCHA, 2021).

In 2021, as many as 41,000 Iranians were displaced as a result of drought, and sand and dust storms (SDSs) (Middle East Institute, 2023), and in Syria a dramatic decrease in rainfall, increasingly hot temperatures, and the destruction of agricultural lands and desertification has displaced 2 million people from rural-urban areas (UNOCHA, 2022). It has also impacted the effective functioning of key infrastructure (e.g., health care facilities), severely constrained agriculture including economic activities in farming and fishing, and increased exposure to wildfires, air pollution, and water-borne diseases such as diarrhoea and cholera, particularly among displaced people in camps and children (Save the Children, 2021).

The semi-arid region affected by the drought is chiefly dependent on rainfall during the extended winter months, roughly from October to April with January to April being particularly important for the growing season. While there is relatively high year-to-year variability in the rainfall, the last three years in particular over the Tigris-Euphrates basin in Syria and Iraq have seen exceptionally low rainfall, following a few years of comparably high rains (see section 3.1) and associated good harvests. Droughts resulting from similarly low rains have only occurred a few times in all of the historic record, such as in the early 2000s over the whole region, and in the 1960s and 1970s in Iran and Iraq (see sec. 3.1). When looking at evaporation as well as rainfall the only comparable event to the current drought was in the early 2000s.

1.1 Event Definition

Increased potential evapotranspiration due to regional warming can play a major role in exacerbating drought impacts, particularly in agriculture, through changes in soil moisture and evapotranspiration rates. Therefore, this study adopts a bivariate approach that assesses the combined effect of rainfall deficit with high temperatures. We use the Standardised Precipitation Evapotranspiration Index (SPEI)

(Fig. 1) that combines rainfall as well as potential evapotranspiration (PET). We examine changes in SPEI in a 36-month period (July 2020 - June 2023) as well as rainfall in the same period. The colour scheme reflects the US Global Drought Monitor drought classifications (D0 - abnormally dry, D1 - moderate, D2 - severe, D3 - extreme, and D4 - exceptional)

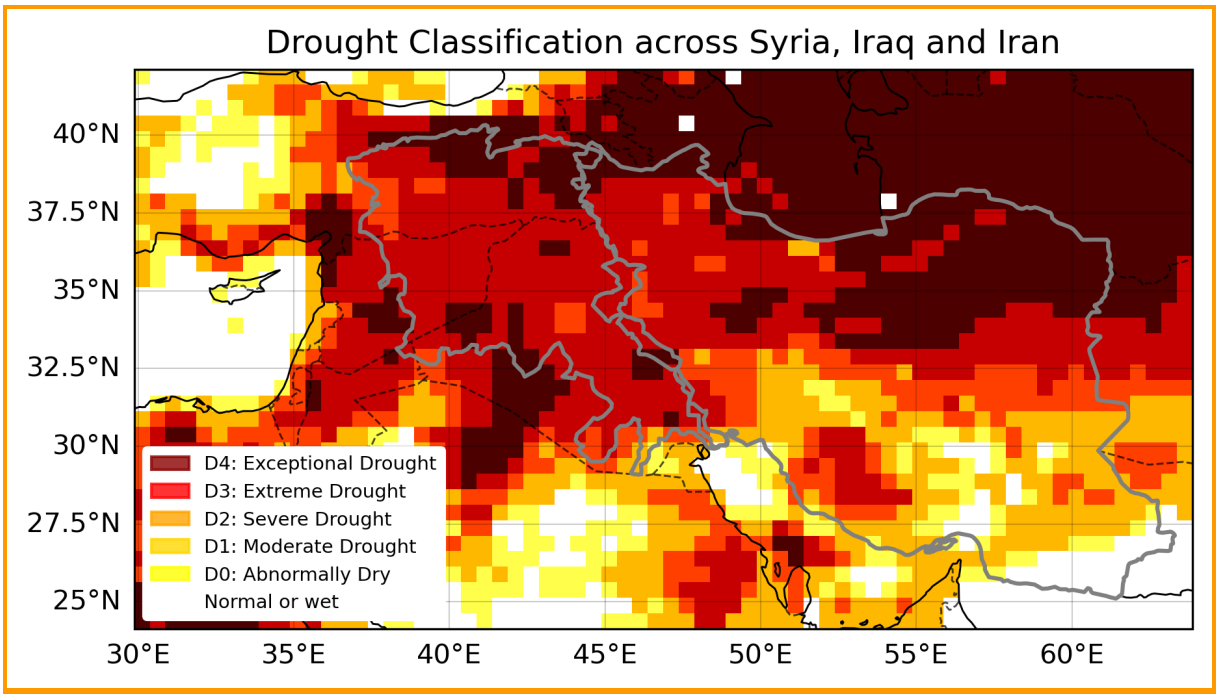

Figure 1: *Drought classification for the wider West Asia region, categorised according to the US Global Drought Monitor system. The categories are based on the 36-month SPEI values in June 2023, calculated from ERA5. The study regions are outlined in grey, the Tigris-Euphrates river basin on the left and Iran to the right.*

To capture the regions facing the worst impacts we look at two regions separately, the Tigris-Euphrates basin over Syria and Iraq, as well as the whole country of Iran. Both regions are outlined in grey in figure 1. While the region has been affected as a whole, the topography is very different over the low lying river basin compared to relatively mountainous Iran. We expect climate models to perform very differently over these two regions and are thus separating them for the analysis.

With annual winter rainfall determining the water balance in both regions, we chose 36 successive months, ending in June 2023, as the temporal event definition. This captures the three years of failed rains modulating the current drought but does not include the new winter season that started in October.

1.2 Background

Attribution studies for droughts or other extreme events in the region are sparse, and information on changing trends that are attributable to human induced climate change generally comes from global attribution studies on temperature and precipitation trends as well as drought indices. Thus IPCC assessment on past changes in extremes is generally ‘low confidence’ for the region (e.g., due to lack

of data and/or lack of peer reviewed papers), apart from an observed increase in agricultural and ecological drought. Only for a 4°C warmer world, an increase in drought is projected for the region as a whole (Seneviratne et al., 2021).

Studies more specifically focussing on the fertile crescent and Syria, thus approximately the same region the Tigris-Euphrates basin captures, have also found an increase in drought frequency and drought severity both for meteorological drought (lack of rainfall) and Palmer-Drought Severity Index PDSI (Kelley et al., 2015). Similar results were obtained by Mathbout et al., (2018) when focussing on Syria alone and calculating SPI and SPEI indices. Rahimi and Fatemi (2019) analysed station data over Iran and found no consistent trend in consecutive dry days and consecutive wet days. Calculating SPI and SPEI for various drought durations over Iran come to similar conclusions with a detectable increase in drought over the central regions and at higher altitudes (Sharafati et al., 2019). Thus, for the region as a whole there is a tendency towards more severe droughts observed as well as projected and the IPCC assessment appears too conservative (Loyd & Oreskes, 2019; Otto et al., 2022) with respect to the countries assessed here. However, trends depend on the exact definition of drought that is looked at. Considering there are no attribution studies on drought and with the region experiencing significant groundwater depletion ((Noori et al., 2023), factors beyond human-induced climate change could be driving trends in hydrological and agricultural drought.

2 Data and methods

2.1 Observational data

The study utilises four observational datasets: ERA5, MSWEP, GPCC and CPC. However CPC is discarded for further analysis.

The European Centre for Medium-Range Weather Forecasts, or the ERA5 reanalysis product begins in the year 1950 and spans to present (Hersbach et al., 2020). We use temperature and rainfall data from this product. It should be noted that the variables from ERA5 are not directly assimilated, but these are generated by atmospheric components of the Integrated Forecast System (IFS) modelling system.

We use CPC daily precipitation. This is the gridded product from NOAA PSL, Boulder, Colorado, USA known as the CPC Global Unified Daily Gridded data, available at 0.5° x 0.5° resolution, for the period 1979-present. Data are available from NOAA.

The Multi-Source Weighted-Ensemble Precipitation (MSWEP) v2.8 dataset (updated from Beck et al., 2019) is fully global, available at 3-hourly intervals and at 0.1° spatial resolution, available from 1979 to ~3 hours from real-time. This product combines gauge-, satellite-, and reanalysis-based data.

We use a combined GPCC product from the Deutscher Wetterdienst, available from the Climate Explorer after merging: i) GPCC Full Data Monthly Product Version 2022 (Schneider et al., 2022), precipitation in mm/month, 1.0 degree, extended with ii) GPCC Monitoring Monthly Product version 2022 (Schneider et al., 2022), precipitation in mm/month, 1.0 degree, extended with iii) GPCC First Guess Product at 1.0 (Ziese et al., 2011): Near Real-Time First Guess Monthly Land-Surface Precipitation from Rain-Gauges based on SYNOP Data combined with the GPCC first guess product.

As a measure of anthropogenic climate change we use the (low-pass filtered) global mean surface temperature (GMST), where GMST is taken from the National Aeronautics and Space Administration (NASA) Goddard Institute for Space Science (GISS) surface temperature analysis (GISTEMP, Hansen et al., 2010 and Lenssen et al. 2019).

2.2 Model and experiment descriptions

We use two multi-model ensembles from climate modelling experiments using very different framings (Philip et al., 2020): Sea Surface temperature (SST) driven global circulation high resolution models, coupled global circulation models and regional climate models.

1. Coordinated Regional Climate Downscaling Experiment CORDEX-CORE over the West-Asia domain with 0.22 km resolution (WAS-22) (Teichman et al., 2021). The ensemble consists of 9 regional climate models, each downscaling 5 GCMs. These simulations are composed of historical simulations up to 2005, and extended to the year 2100 using the RCP8.5 scenario.

2. CMIP6. This consists of simulations from 12 participating models with varying resolutions. For more details on CMIP6, please see Eyring et al., (2016). For all simulations, the period 1850 to 2015 is based on historical simulations, while the SSP5-8.5 scenario is used for the remainder of the 21st century.

2.3 Statistical methods

In this analysis we analyse time series from the Tigris-Euphrates basin and Iran of 36-month SPEI values where long records of observed data are available. We also decompose the meteorological drivers of drought by analysing the trends in both accumulated precipitation and average temperatures over the two regions. Methods for observational and model analysis and for model evaluation and synthesis are used according to the World Weather Attribution Protocol, described in Philip et al. (2020), with supporting details found in van Oldenborgh et al. (2021), Ciavarella et al. (2021) and here.

The analysis steps include: (i) trend calculation from observations; (ii) model evaluation; (iii) multi-method multi-model attribution and (iv) synthesis of the attribution statement.
We calculate the return periods, Probability Ratio (PR; the factor-change in the event's probability) and change in intensity of the event under study in order to compare the climate of now and the climate of the past, defined respectively by the GMST values of now and of the preindustrial period (1850-1900, based on the Global Warming Index). To statistically model the event under study, we use a Gaussian distribution with GMST as a covariate. The results from observations and models that pass the evaluation tests are synthesized into a single attribution statement (sec. 6).

2.3.1. Exceptions in methods

1. **Analysis of 36-month rainfall and drought severity** - Previous studies examining changes in water availability and evapotranspiration rates due to climate change over the West Asia found that warming has resulted in increasing trends the potential for atmospheric water demand (or Potential evapotranspiration (PET)) in these parts, which will continue to increase

under future warming (Ajjur and Ghamdi., 2021; Al-Hasani and Shahid, 2022). Given the implications of increasing evaporative demand in exacerbating droughts (Karimi et al., 2020; Salman et al., 2020), we supplement the standard univariate analysis of the 36-month precipitation in the study regions with an analysis of the joint changes in the 36-month precipitation and PET using copulas, following Zachariah et al., 2023 and Zscheischler and Lehner, 2022).

(i) We fit Gaussian distributions that scale and shift with GMST to the observed 36-month precipitation (X) and the 36-month accumulated PET (Y) time series respectively:

$$X \sim normal(\mu_X, \sigma_X, \alpha_X) \quad \text{and} \quad Y \sim normal(\mu_Y, \sigma_Y, \alpha_Y).$$

(ii) We use the cumulative distribution functions (CDFs) of these two distributions to compute the probabilities u and v of exceeding the values observed at each time t, so that

$$u_t = P(X \leq x_t) \quad \text{and} \quad v_t = 1 - P(Y \leq y_t)$$

Note that, because we are interested in the lower tails of the precipitation distribution and the upper tails of the PET distribution, these exceedance probabilities are given by the CDF of X and 1 - the CDF of Y.

(ii) The joint cumulative distribution function C is estimated from the marginal exceedance probabilities u and v by fitting a stationary Student's-t copula such that $C(\{u\},\{v\}) = P(\{U \leq u\},\{V \leq v\})$ for all (u, v) pairs (Nelsen, 2006).

(iv) Contours can be plotted over the subset $\{u, v\} \subset \{U, V\}$ - and therefore over the subset $\{x, y\} \subset \{X, Y\}$ - that share the same joint exceedance probability p, where $1/p$ is the return period of the event.

(v) The univariate distributions fitted in Step (i) are used to transform the (u,v) pairs to their equivalent return levels in the current climate and in a 1.2°C cooler climate in order to obtain joint return period contours for the current and pre-industrial climates.

3 Observational analysis: return period and trend

3.1 Precipitation

Figure 2 shows time series for accumulated precipitation for the regions of interest. Three out of the four available data sets show good agreement despite differences in the magnitude, the exception being CPC that exhibits different behaviour, especially towards the beginning of the time series where the magnitude and variability is much lower, while it is comparable towards recent years. Hence, any trend assessment using CPC will reflect this, which presumably is an artefact of data availability rather than a real trend. Further, GPCC and MSWEP only have data back to 1980, which is not long enough to reliably show trends in a 3-year metric. We thus exclude CPC, MSWEP and GPCC from further assessment. The time series also shows that both regions had a few years of comparably high

rainfall prior to the present drought, while similarly dry years have occurred at the beginning of the 21st century as well as around the year 1990.

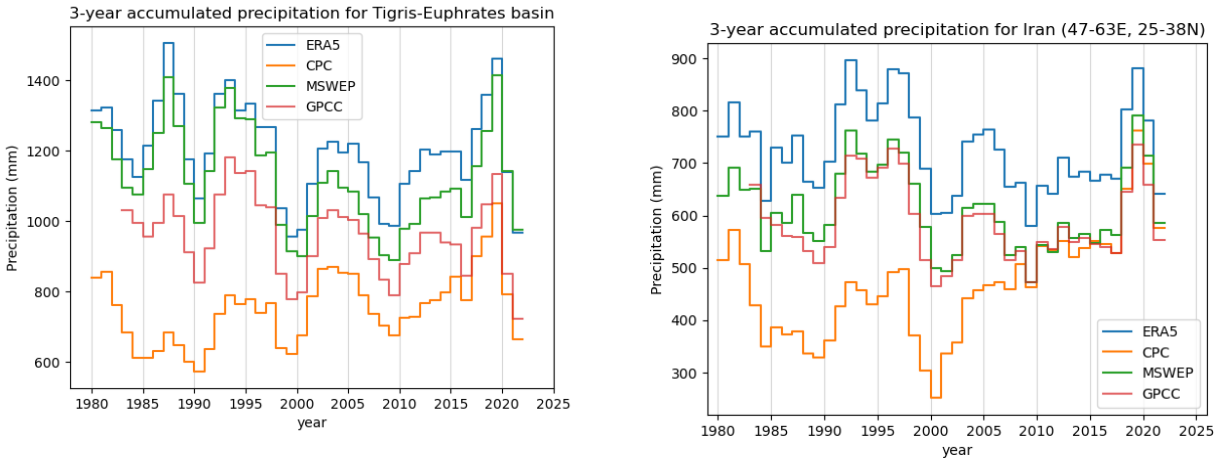

Figure 2: *3-year accumulated precipitation over the Tigris-Euphrates Basin (left) and Iran (right) in four different observation based data sets, CPC, GPCC, MSWEP and ERA5. Data is shown for the period of 1980 onwards, corresponding to the period in which all datasets have records.*

Analysis of the trends in the 36-month accumulated precipitation in the two study regions show that rainfall has been decreasing due to global warming, although the trend is not significant (see Fig. A1(a-b)). Fig. A1 (c-d) shows the results from the trend-fitting method described in Philip et al. (2020) applied to the 36 month accumulated precipitation in the two domains. The return period of the 2020-23 event is found to be 1-in-25 years (uncertainty: ~10-100). The best estimates for the probability ratio with respect to the hypothetical 1.2℃ cooler climate is ~1 for Iran and ~2 for the Tigris-Euphrates basin, along with 2-3% decrease in rainfall. However the uncertainty bounds for these estimates encompass no change, indicating that these estimates are not statistically significant.

As has been demonstrated in previous studies for the larger region (as explained in Section 2.3.1), the impacts of droughts are not driven by rainfall deficits alone. Rising temperatures via increased PET affect evapotranspiration rates and agriculture. Therefore we focus on SPEI as the primary indicator for analysing this drought event. The results are discussed in the following section.

3.2 SPEI

Considering the role of increased PET associated with regional warming in amplifying drought impacts, especially agriculture due to changes in soil moisture and evapotranspiration rates, we also compute the trends and climate change signals in the 36-month SPEI. As there are several different methods to calculate PET, often with large differences, we first test the sensitivity of SPEI estimates to different methods of calculating PET. In water-stressed regions, PET is often greater than actual evapotranspiration as the latter is limited by lack of moisture in the soils. Therefore for areas where latent heat fluxes are or will become limited by moisture supply, PET is expected to increase more than actual evapotranspiration (Jung et al., 2010).

The choice of the PET estimation method in calculating any drought index is subjective but is also limited by the availability of meteorological data and the climatic conditions of the region (Trajkovic et al., 2010; Tabari et al., 2013; Zhao et al., 2021). Several studies (Begueria et al., 2014; Van der Schrier et al., 2011; Dai 2011; Sheffield et al., 2012) have compared and evaluated the effect of using different PET equations in the calculation of drought indices. While most of these studies recommend methods that factor radiative and aerodynamic processes (e.g, FAO Penman–Monteith; Allen et al., 1998) in preference to those that consider temperature as the main input (e.g., Thornthwaite; (Thornthwaite (1948), and Hargreaves-Samani; Hargreaves and Samani, 1985), such methods require several climatic parameters that are often unavailable in developing countries, especially in remote arid and semi-arid regions. We thus only employ temperature based methods: Hargreaves (Hargreaves and Samani, 1982;Hargreaves and Samani, 1985), Baier-Robertson (Baier and Robertson, 1965) and Thornthwaite (Thornthwaite (1948), as well as the direct PET output of ERA5. The latter is based on surface energy calculations assuming "crops/mixed farming" for the vegetation parameters, that evaporation is not limited by surface water availability, and that the atmosphere is unaffected by this artificial condition (Vicente-Serrano et al., 2022; Copernicus, 2023). We note that this set of assumptions is known to give unrealistic values in arid regions, which makes up part of each of our regions. Nonetheless, we find results to be fairly similar in both regions for the 36-months SPEI values in June 2023 (table 1).

Table 1: *SPEI-36 magnitudes and trends (per 1.2 C of GMST change) for June 2023 for different PET methods. Reported SPEIbase values are calculated from the 10- and 5- year return period for each region, respectively.*

PET calculation method	**Tigris-Euphrates**		**Iran**	
	Magnitude	Magnitude change	Magnitude	Magnitude change
Hargreaves	-1.94	-1.28	-1.85	-1.42
Baier and Robertson	-1.98	-1.40	-1.85	-1.58
Thornthwaite	-2.19	-3.06	-2.00	-2.62
ERA5 PET	-2.05	-1.77	-2.01	-2.07
SPEIbase	-2.29	-2.09	-1.92	-1.92

We also compare the SPEI values resulting from these methods and the Global SPEI database 'SPEIbase', which uses the Penman-Monteith formulation of PET and thus forms our benchmark (table 1). The Thornthwaite method shows a much stronger trend than other methods and gives the highest event magnitudes. We therefore eliminate this method from further use. One issue with all temperature-based methods is the potential to result in unphysical levels of potential evaporation based on ultimately limited radiation. However, the SPEIbase method uses radiative inputs, and results in a stronger magnitude and trend than the remaining temperature-based methods. This reinforces our confidence that the temperature-based methods used for this analysis provide reasonable estimates. Furthermore, while Hargreaves and Baier-Robertson are slightly wetter than the SPEIbase dataset, they are otherwise comparable in both trend and event magnitudes (Fig. 3 table 1). As a result, we use the Hargreaves method throughout the following assessment.

The observed SPEI values in the ERA5 dataset using the Hargreaves estimate method are -1.94 and -1.85 for the two regions respectively. We employ a drought classification system in accordance with the US Global Drought Monitor, in which SPEI values greater than -0.5 are 'normal or wet conditions'; -0.5 to -0.8 are abnormally dry (D0); -0.8 to -1.3 are moderate drought (D1); -1.3 to -1.6 are severe drought (D2); -1.6 to -2 are extreme drought (D3); and values less than -2 are exceptional drought (D4). Both events in today's climate are classified as extreme droughts (D3).

We standardise the SPEI values with respect to the 1980 to 2010 climatology. The return period of this event in the current climate is 9 years (4.79 – 25.76) for the Tigris-Euphrates region and 7 years (4.19 - 15.95) over Iran. For both cases the event has been made more likely due to human-induced climate change. For the Tigris-Euphrates basin, the probability ratio is 19.93 (3.36 – 257.52), which corresponds to a change in intensity of -1.28 (-2.11 - - 0.49). In other words, without climate change the SPEI for this event would be -0.66, falling into the category of abnormally dry (D0) and thus could not be classified as drought conditions with respect to the 1980-2010 climatology. For Iran the probability ratio is 40.22 (5.56 - 857.12) and the intensity change is -1.42 (-2.1 - -0.71) corresponding to an SPEI of -0.43 in the 1.2°C cooler climate, which also would be categorised as normal conditions with respect to the 1980-2010 climatology.

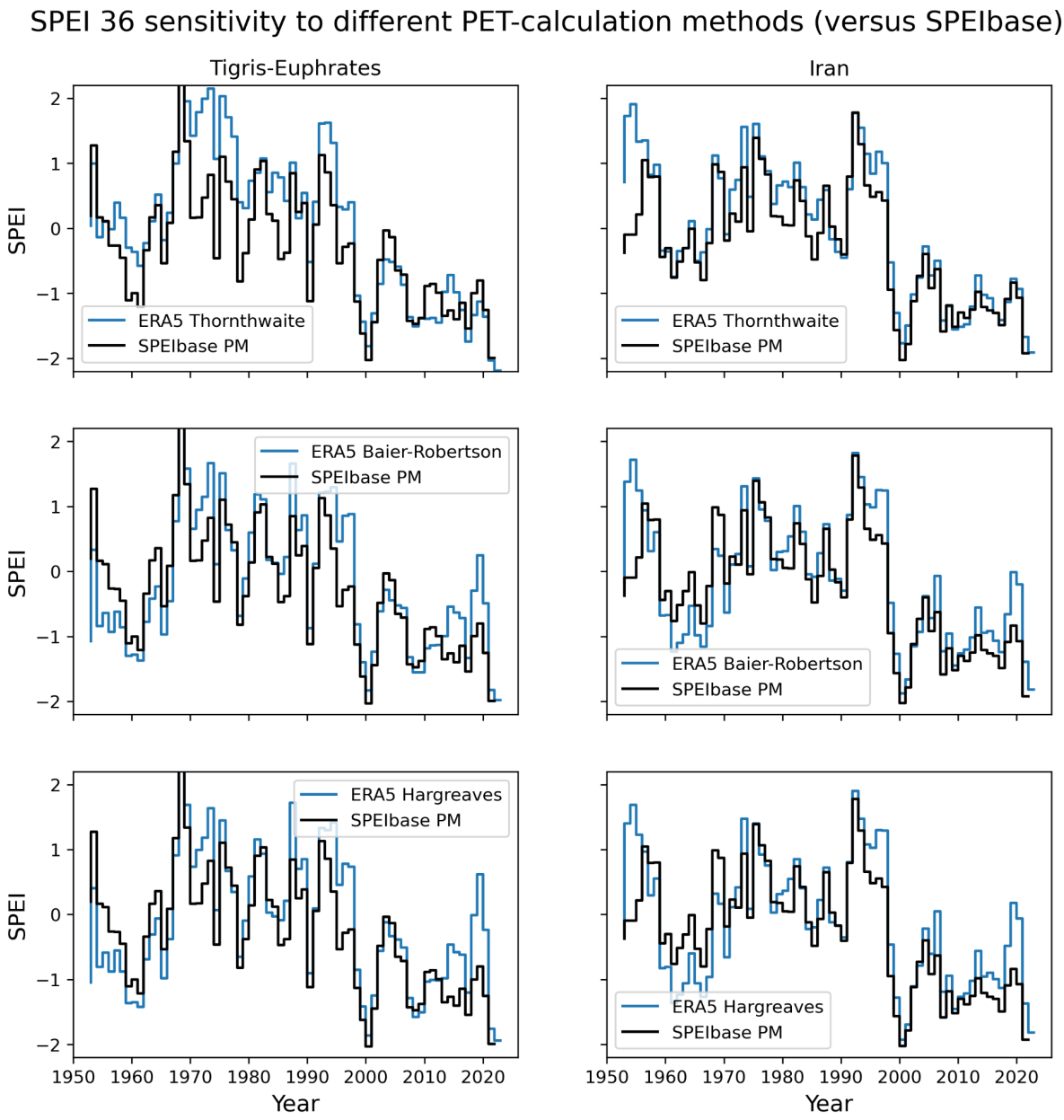

Figure 3: *36-month SPEIs calculated using ERA5 data and various methods for estimating PET: Thornthwaite (top), Baier-Robertson (middle), Hargreaves (bottom), across the two regions the Tigris-Euphrates basin (left) and Iran (right). ERA-based estimates are in blue, while SPEIbase (black) is used as the comparison in each case. The years are the same for all 6 graphs.*

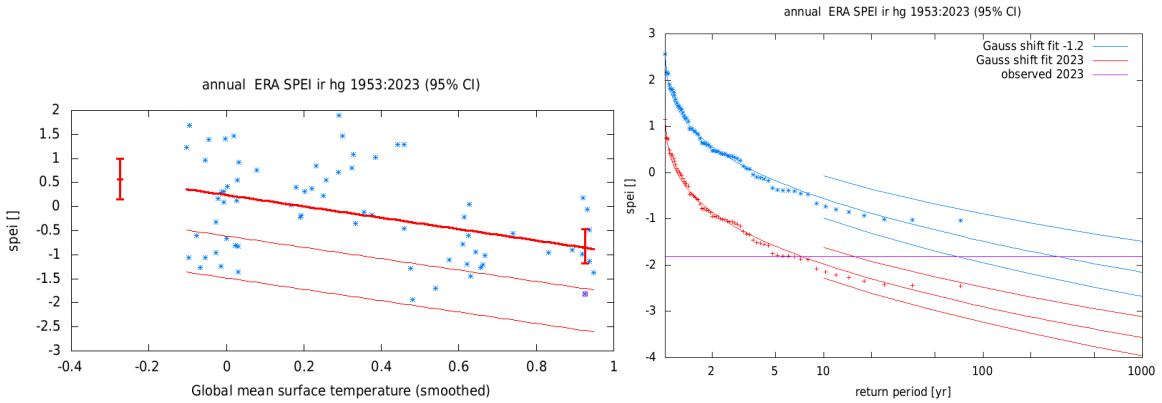

Figure 4, Left: *Annual SPEI calculated over Iran. The thick red line denotes the time-varying mean, and the thin lines show 1 standard deviation (s.d) and 2 s.d below. The vertical red lines show the 95% confidence interval for the location parameter, for the 2023 climate and the hypothetical 1.2ºC cooler climate. The 36-month SPEI calculated in June 2023 is given by the magenta box.* ***Right:*** *Gaussian return periods of 36-month SPEI for the 2023 climate (red lines) and the 1.2ºC cooler climate (blue lines with 95% CI), calculated using the Hargreaves method from temperatures and precipitation in the ERA5 dataset.*

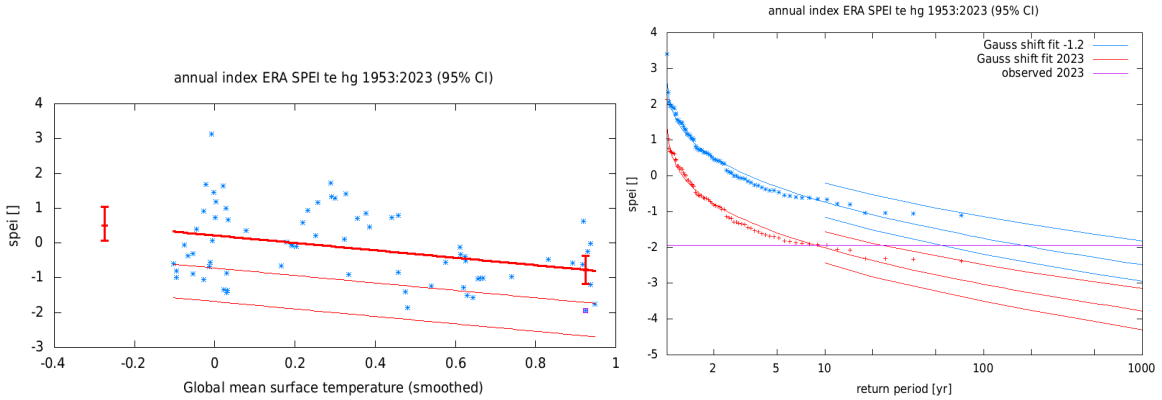

Figure 5, Left: *Annual SPEI calculated over the Tigris-Euphrates region. The thick red line denotes the time-varying mean, and the thin lines show 1 standard deviation (s.d) and 2 s.d below. The vertical red lines show the 95% confidence interval for the location parameter, for the current 2023 climate and the hypothetical 1.2ºC cooler climate. The 36-month SPEI calculated in June 2023 is given by the magenta box.* ***Right:*** *Gaussian return periods of 36-month SPEI for the 2023 climate (red lines) and the 1.2ºC cooler climate (blue lines with 95% CI), calculated using the Hargreaves method from temperatures and precipitation in the ERA5 dataset.*

The coloured areas in Figure 6 show the 36-month SPEI drought classification (standardised with respect to the 1981-2010 climatology) corresponding to a range of values of 36-month accumulated precipitation and PET. The solid lines are contours representing pairs of precipitation and PET values that have equal probability of occurring in the 2023 climate in the joint distribution of precipitation and PET (see Section 2.3.1 for details), labelled with the corresponding return period; the magenta dot represents the combination of precipitation and PET observed in 2023. The dotted lines represent contours of the joint distribution of precipitation and PET in a 1.2°C cooler climate, with the turquoise dot indicating an event in the 1.2°C cooler climate of the same rarity as the 2023 event. In both regions (Tigris-Euphrates and Iran), the shift in the joint distribution (and hence in drought severity) is largely the result of a large increase in PET. In the current climate, this combination of precipitation

and PET has a joint return time of 84 years in the Tigris-Euphrates basin and 29 years in Iran, and in both cases classified as an extreme drought (class D3) with respect to the 1981-2010 climatology. Precipitation and PET of comparable rarity in a 1.2°C cooler climate would have resulted in conditions considered a severe and moderate drought with respect to the 1980-2010 climatology, respectively, in the Tigris-Euphrates basin and Iran.

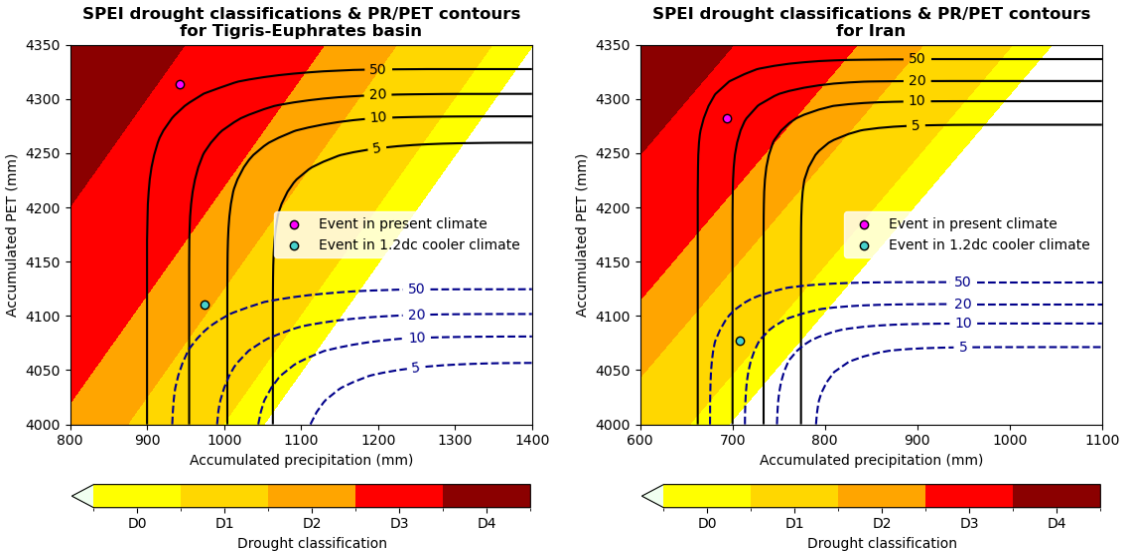

Figure 6, Left: *Joint distribution of 36-month precipitation and PET with corresponding SPEI drought classification (ERA5 dataset) for Tigris-Euphrates basin. The solid contours indicate return periods under the joint distribution in the current climate, while the dashed contours indicate the same return periods in a 1.2°C cooler climate. The shaded contours represent different levels of drought severity (D0-D4). The magenta point indicates the accumulated precipitation and PET observed in 2023, with this particular combination of precipitation and PET having a joint return period of 84 years; the turquoise point shows an event of equivalent rarity in a 1.2°C cooler climate.*
Right: *As Left, but for Iran, where the observed combination of precipitation and PET has a return time of 29 years in the current climate.*

It is important to highlight that the drought categories from the joint distribution are not equivalent to the ones predicted by the linear model depicted above (Fig. 4 & 5) and used in all other analyses in this study. This is because the contour plots (Fig 6) only consider this particular combination of precipitation and PET, while the linear model considers any combination of precipitation and PET leading to this SPEI value.

Finally, we also analyse the trends in the 36-month average temperatures in these regions. With return periods of 1-in-15 years (uncertainty: 7-55) and 1-in-4 years (uncertainty:3-11) in the Tigris-Euphrates basin and in Iran respectively, the 2020-23 observed temperatures would not have occurred in the pre-industrial climate (PR tends to inf) and were made 2-3°C warmer due to climate change (Appendix Fig. A2).

4 Model evaluation

We evaluated the climate models against the observations in their ability to capture the seasonal cycles, spatial patterns (see fig A7-A9), and the parameters of the fitted models. For the seasonal cycle, we qualitatively compare the model outputs against observations-based plots. We discard the

models that fail to capture the unimodal seasonal cycle and/or exhibit ill-defined peaks in their seasonal cycles. We also discard the model if the start of the rainy season varies significantly from the observations. For spatial patterns, models that do not match the observations in terms of the large-scale precipitation and temperature patterns are excluded. For model parameters, we exclude any model whose parameter ranges do not overlap with those derived from observations. For distributions that scale with GMST (such as the precipitation-based indices in this study) we evaluate the dispersion parameter, while for those that shift with GMST (in this case, temperature) we assess the variance parameter (Philip et al., 2020). Based on their performance across these three criteria, models are categorised as 'good,' 'reasonable,' or 'bad.' Per framing or model setup, we also use models that only just pass the evaluation tests if we only have five models or less for that framing that perform well. Due to limitations in observed evapotranspiration products we do not evaluate the models for effective precipitation. Instead, for the SPEI attribution analysis we choose those models that pass the evaluation for both precipitation and temperature. Tables 2 and 3 show the model evaluation results.

4.1 Iran

Table 2: *Evaluation results for the climate models considered for the attribution analysis of* ***36-month SPEI, precipitation and temperature.****. The table contains qualitative assessments of seasonal cycle and spatial pattern of SPEI, precipitation and temperature from the models (good, reasonable, bad) along with estimates for dispersion parameter and event magnitude for SPEI. The corresponding estimates for observations are shown in blue. Based on overall suitability, the models are classified as good, reasonable and bad, shown by green, yellow and red highlights, respectively. As the table combines all variables there is no green entry as no model performance is labelled "good" over all criteria in all three variables.*

Observations	**Precipitation**		**Temperature**		**SPEI-36**	
	Seasonal cycle	**Spatial pattern**	**Seasonal cycle**	**Spatial pattern**	**Dispersion**	**Event magnitude [SPEI]**
ERA5					0.879 (0.745 ... 0.985)	-1.82
ERA5 – precalculated PET					0.848 (0.727 ... 0.947)	-1.92
SPEIbase					0.684 (0.570 ... 0.787)	-1.92
Model						**Threshold for 5-yr return period**
CMIP6						
ACCESS-ESM1-5_ssp585_r1i1p1f1	reasonable	reasonable	good	good	1.08 (0.874 ... 1.22)	-2.1171715
CMCC-ESM2_ssp585_r1i1p1f1	reasonable	reasonable	good	good	1.33 (1.02 ... 1.56)	-0.9783134

EC-Earth3_ssp585_r1i1p1f1	reasonable	good	good	good	0.870 (0.706 ... 0.988)	-1.0893538
EC-Earth3-Veg-LR_ssp585_r1i1p1f1	reasonable	reasonable	good	good	0.964 (0.781 ... 1.08)	-0.9112214
GFDL-CM4_ssp585_r1i1p1f1	reasonable	reasonable	good	good	1.12 (0.930 ... 1.26)	-3.6634493
IPSL-CM6A-LR_ssp585_r1i1p1f1	reasonable	reasonable	good	good	0.870 (0.666 ... 1.02)	-1.4638538
KACE-1-0-G_ssp585_r1i1p1f1	good	reasonable	good	good	0.799 (0.637 ... 0.933)	-2.0768382
MIROC6_ssp585_r1i1p1f1	reasonable	reasonable	good	good	0.963 (0.785 ... 1.08)	-0.7141277
MRI-ESM2-0_ssp585_r1i1p1f1	reasonable	good	good	good	0.916 (0.714 ... 1.07)	-1.1149383
NorESM2-LM_ssp585_r1i1p1f1	reasonable	reasonable	good	good	1.00 (0.826 ... 1.12)	-1.4887672
NorESM2-MM_ssp585_r1i1p1f1	reasonable	good	good	good	0.965 (0.770 ... 1.11)	-0.2764717
TaiESM1_ssp585_r1i1p1f1	reasonable	good	good	good	1.01 (0.780 ... 1.15)	-1.8463435
CORDEX						
EC-EARTH_r12_CLMcom-ETH-COSMO-crCLIM-v1-1	reasonable	reasonable	good	good	1.09 (0.859 ... 1.25)	-1.3707272
HadGEM2-ES_r1_GERICS-REMO2015	bad	good	good	good	0.941 (0.726 ... 1.10)	-0.2170235
MIROC5_r1_ICTP-RegCM4-7	good	bad	good	good	0.752 (0.553 ... 0.890)	0.89597869
MPI-ESM-LR_r1_CLMcom-ETH-COSMO-crCLIM-v1-1	reasonable	good	good	good	0.977 (0.829 ... 1.08)	-0.9072819
MPI-ESM-LR_r1_GERICS-REMO2015	reasonable	good	good	good	0.990 (0.814 ... 1.10)	-0.3480741
MPI-ESM-MR_r1_ICTP-RegCM4-7	bad	bad	good	good	0.923 (0.730 ... 1.07)	-0.7392845
NorESM1-M_r1_CLMcom-ETH-COSMO-crCLIM-v1-1	reasonable	reasonable	good	good	1.20 (0.926 ... 1.39)	-1.1915413
NorESM1-M_r1_GERICS-REMO2015	reasonable	good	good	good	1.27 (0.981 ... 1.47)	-1.5445934
NorESM1-M_r1_ICTP-RegCM4-7	reasonable	bad	good	good	0.983 (0.784 ... 1.13)	-0.41108

4.2 Tigris-Euphrates basin

Table 3: *As table 2 but for the Tigris-Euphrates basin.*

Observations	Precipitation	Temperature	SPEI-36	

	Seasonal cycle	Spatial pattern	Seasonal cycle	Spatial pattern	Dispersion	Event magnitude [SPEI]
ERA5					0.969 (0.808 ... 1.10)	-1.94
ERA5 – precalculated PET					0.932 (0.789 ... 1.07)	-2.05
SPEIbase					0.716 (0.568 ... 0.839)	-2.29
Model						**Threshold for 10-yr return period**
CMIP6						
ACCESS-ESM1-5_ssp585_r1i1p1f1	reasonable	reasonable	good	good	1.06 (0.803 ... 1.27)	-1.44
CMCC-ESM2_ssp585_r1i1p1f1	good	reasonable	good	good	1.18 (0.958 ... 1.32)	-1.71
EC-Earth3_ssp585_r1i1p1f1	reasonable	good	good	good	0.926 (0.720 ... 1.08)	-1.79
EC-Earth3-Veg-LR_ssp585_r1i1p1f1	reasonable	reasonable	good	good	1.00 (0.786 ... 1.17)	-1.70
GFDL-CM4_ssp585_r1i1p1f1	good	reasonable	good	good	1.11 (0.871 ... 1.28)	-2.58
IPSL-CM6A-LR_ssp585_r1i1p1f1	reasonable	reasonable	good	good	0.895 (0.697 ... 1.04)	-1.55
KACE-1-0-G_ssp585_r1i1p1f1	good	reasonable	good	good	0.663 (0.523 ... 0.761)	-2.29
MIROC6_ssp585_r1i1p1f1	good	reasonable	good	good	1.15 (0.898 ... 1.34)	-1.87
MRI-ESM2-0_ssp585_r1i1p1f1	reasonable	good	good	good	1.14 (0.887 ... 1.34)	-2.88
NorESM2-LM_ssp585_r1i1p1f1	reasonable	reasonable	good	good	0.876 (0.700 ... 1.01)	-4.89
NorESM2-MM_ssp585_r1i1p1f1	reasonable	good	good	good	0.981 (0.830 ... 1.08)	-1.05
TaiESM1_ssp585_r1i1p1f1	reasonable	good	good	good	0.884 (0.659 ... 1.06)	-3.78
CORDEX						
EC-EARTH_r12_CLMcom-ETH-COSMO-crCLIM-v1-1	good	reasonable	good	good	1.07 (0.892 ... 1.18)	-1.64
HadGEM2-ES_r1_GERICS-REMO2015	reasonable	good	good	good	0.922 (0.708 ... 1.06)	-1.12
MIROC5_r1_ICTP-RegCM4-7	good	bad	good	good	0.644 (0.478 ... 0.755)	0.71
MPI-ESM-LR_r1_CLMcom-ETH-COSMO-crCLIM-v1-1	good	good	good	good	0.991 (0.793 ... 1.11)	-1.43

MPI-ESM-LR_r1_GERICS-REMO2015	reasonable	good	good	good	1.01 (0.804 ... 1.15)	-1.39
MPI-ESM-MR_r1_ICTP-RegCM4-7	good	bad	good	good	0.924 (0.734 ... 1.07)	-1.62
NorESM1-M_r1_CLMcom-ETH-COSMO-crCLIM-v1-1	good	reasonable	good	good	0.960 (0.768 ... 1.10)	-0.97
NorESM1-M_r1_GERICS-REMO2015	good	good	good	good	1.04 (0.848 ... 1.17)	-1.45
NorESM1-M_r1_ICTP-RegCM4-7	bad	bad	good	good	1.00 (0.819 ... 1.16)	-0.88

5 Multi-method multi-model attribution

For models that pass the evaluation test (see section 2.4), we calculate Probability Ratios (PR) and change in intensity (ΔI) for the 36-month SPEI. In this section, we show PR and ΔI results for the selected climate models along with observations-based products.

5.1 Iran

Table 4: *Probability ratio and change in intensity in the* ***36-month SPEI*** *for models that passed the evaluation tests over Iran.*

Model / Observations	Past-Present		Present-Future	
	Probability ratio PR [-]	Change in intensity ΔI [SPEI]	Probability ratio PR [-]	Change in intensity ΔI [SPEI]
ERA5	40 (5.6 ... 8.6e+2)	-1.4 (-2.1 ... -0.71)		
ERA5-precalculated PE	4.8e+2 (48 ... 2.0e+4)	-2.1 (-2.7 ... -1.4)		
SPEIbase	3.8e+3 (3.8e+2 ... 1.8e+5)	-1.9 (-2.2 ... -1.7)		
CMCC-ESM2_ssp585_r1i1p1f1 historical-ssp585 (1)	1.6 (0.74 ... 3.2)	-0.37 (-0.95 ... 0.21)	1.7 (1.5 ... 1.8)	-0.80 (-1.0 ... -0.57)
EC-Earth3_ssp585_r1i1p1f1 historical-ssp585 (1)	3.4 (1.7 ... 6.4)	-0.62 (-0.96 ... -0.24)	1.9 (1.7 ... 2.1)	-0.51 (-0.61 ... -0.38)
EC-Earth3-Veg-LR_ssp585_r1i1p1f1 historical-ssp585 (1)	2.2 (0.99 ... 4.6)	-0.46 (-0.88 ... 0.0033)	1.7 (1.6 ... 1.9)	-0.65 (-0.78 ... -0.48)
GFDL-CM4_ssp585_r1i1p1f1 historical-ssp585 (1)	1.1e+3 (3.0e+2 ... 5.6e+3)	-4.0 (-4.6 ... -3.3)	6.7 (5.3 ... 9.5)	-2.1 (-2.3 ... -1.9)
IPSL-CM6A-LR_ssp585_r1i1p1f1 historical-ssp585 (1)	9.9 (5.4 ... 20)	-1.1 (-1.5 ... -0.81)	2.5 (2.2 ... 2.9)	-0.88 (-0.97 ... -0.78)
KACE-1-0-G_ssp585_r1i1p1f1 historical-ssp585 (1)	33 (17 ... 71)	-1.4 (-1.7 ... -1.1)	3.5 (3.0 ... 4.4)	-0.63 (-0.72 ... -0.54)
MIROC6_ssp585_r1i1p1f1 historical-ssp585 (1)	0.53 (0.21 ... 1.2)	0.56 (-0.20 ... 1.3)	1.4 (1.2 ... 1.4)	-0.69 (-1.1 ... -0.28)
MRI-ESM2-0_ssp585_r1i1p1f1 historical-ssp585 (1)	1.2 (0.60 ... 2.1)	-0.12 (-0.59 ... 0.37)	1.3 (1.1 ... 1.5)	-0.28 (-0.49 ... -0.040)

NorESM2-LM_ssp585_r1i1p1f1 historical-ssp585 (1)	5.6 (1.5 ... 30)	-1.1 (-1.9 ... -0.23)	2.1 (1.9 ... 2.5)	-1.2 (-1.5 ... -0.98)
NorESM2-MM_ssp585_r1i1p1f1 historical-ssp585 (1)	0.83 (0.27 ... 2.1)	0.11 (-0.47 ... 0.68)	1.5 (1.4 ... 1.6)	-0.64 (-0.87 ... -0.44)
EC-EARTH_r12_CLMcom-ETH-COSMO-crCLIM-v1-1 historical-rcp85 (1)	1.6 (0.42 ... 5.7)	-0.34 (-1.2 ... 0.60)	1.4 (0.97 ... 1.8)	-0.31 (-0.61 ... 0.023)
MPI-ESM-LR_r1_CLMcom-ETH-COSMO-crCLIM-v1-1 historical-rcp85 (1)	1.3 (0.51 ... 3.2)	-0.20 (-0.82 ... 0.40)	1.5 (1.2 ... 1.8)	-0.41 (-0.64 ... -0.17)
MPI-ESM-LR_r1_GERICS-REMO2015 historical-rcp85 (1)	0.39 (0.096 ... 1.1)	0.83 (-0.083 ... 1.6)	1.1 (0.81 ... 1.3)	-0.11 (-0.41 ... 0.20)
NorESM1-M_r1_CLMcom-ETH-COSMO-crCLIM-v1-1 historical-rcp85 (1)	2.5 (0.51 ... 14)	-0.65 (-1.8 ... 0.38)	1.8 (1.4 ... 2.2)	-0.61 (-0.95 ... -0.26)
NorESM1-M_r1_GERICS-REMO2015 historical-rcp85 (1)	3.2 (0.32 ... 39)	-0.85 (-2.5 ... 0.71)	1.3 (0.80 ... 2.0)	-0.25 (-0.64 ... 0.15)

5.2 Tigris-Euphrates Basin

Table 5: *Probability ratio and change in intensity in the* ***36-month SPEI*** *for models that passed the evaluation tests over Tigris-Euphrates basin.*

	Past-Present		**Present-Future**	
Model / Observations	**Probability ratio PR [-]**	**Change in intensity ΔI []**	**Probability ratio PR [-]**	**Change in intensity ΔI []**
ERA5	20 (3.4 ... 2.6e+2)	-1.3 (-2.1 ... -0.49)		
ERA5-precalculated PE	1.1e+2 (18 ... 2.2e+3)	-1.8 (-2.5 ... -1.1)		
SPEIbase	7.5e+3 (4.7e+2 ... 7.8e+5)	-2.1 (-2.6 ... -1.6)		
ACCESS-ESM1-5_ssp585_r1i1p1f1 historical-ssp585 (1)	1.2 (0.42 ... 3.4)	-0.14 (-0.83 ... 0.53)	1.5 (1.3 ... 1.8)	-0.44 (-0.69 ... -0.21)
CMCC-ESM2_ssp585_r1i1p1f1 historical-ssp585 (1)	10 (4.2 ... 27)	-1.2 (-1.8 ... -0.64)	3.1 (2.7 ... 3.7)	-1.0 (-1.2 ... -0.86)
EC-Earth3_ssp585_r1i1p1f1 historical-ssp585 (1)	5.1 (2.0 ... 12)	-0.71 (-1.1 ... -0.29)	2.3 (1.9 ... 2.7)	-0.54 (-0.67 ... -0.39)
EC-Earth3-Veg-LR_ssp585_r1i1p1f1 historical-ssp585 (1)	2.5 (0.97 ... 6.4)	-0.58 (-1.1 ... 0.024)	2.0 (1.7 ... 2.4)	-0.82 (-1.1 ... -0.51)
GFDL-CM4_ssp585_r1i1p1f1 historical-ssp585 (1)	54 (13 ... 2.8e+2)	-1.8 (-2.4 ... -1.1)	4.5 (3.7 ... 5.8)	-1.2 (-1.3 ... -1.0)
IPSL-CM6A-LR_ssp585_r1i1p1f1 historical-ssp585 (1)	7.3 (3.7 ... 18)	-0.91 (-1.3 ... -0.58)	2.8 (2.4 ... 3.4)	-0.77 (-0.87 ... -0.67)
KACE-1-0-G_ssp585_r1i1p1f1 historical-ssp585 (1)	67 (28 ... 2.0e+2)	-1.3 (-1.6 ... -1.0)	4.8 (3.9 ... 6.6)	-0.77 (-0.86 ... -0.68)
MIROC6_ssp585_r1i1p1f1 historical-ssp585 (1)	0.74 (0.17 ... 2.4)	0.22 (-0.67 ... 1.1)	1.8 (1.6 ... 2.0)	-0.83 (-1.0 ... -0.60)
MRI-ESM2-0_ssp585_r1i1p1f1 historical-ssp585 (1)	12 (4.3 ... 43)	-1.5 (-2.2 ... -0.84)	2.4 (1.9 ... 3.1)	-0.87 (-1.2 ... -0.51)
NorESM2-LM_ssp585_r1i1p1f1 historical-ssp585 (1)	1.1e+5 (8.9e+3 ... 4.1e+6)	-7.3 (-8.3 ... -6.3)	15 (10 ... 23)	-4.2 (-4.6 ... -3.9)

NorESM2-MM_ssp585_r1i1p1f1 historical-ssp585 (1)	6.9 (1.4 ... 34)	-0.67 (-1.2 ... -0.098)	2.6 (2.3 ... 3.1)	-0.85 (-1.0 ... -0.68)
TaiESM1_ssp585_r1i1p1f1 historical-ssp585 (1)	2.3e+2 (79 ... 9.4e+2)	-2.7 (-3.3 ... -2.2)	5.7 (4.3 ... 8.6)	-1.1 (-1.2 ... -0.95)
EC-EARTH_r12_CLMcom-ETH-COSMO-crCLIM-v1-1 ()	1.2 (0.21 ... 4.6)	-0.092 (-0.85 ... 0.84)	0.78 (0.48 ... 1.1)	0.19 (-0.10 ... 0.49)
HadGEM2-ES_r1_GERICS-REMO2015 ()	0.71 (0.19 ... 2.5)	0.20 (-0.48 ... 0.84)	1.4 (1.0 ... 1.8)	-0.24 (-0.43 ... -0.027)
MPI-ESM-LR_r1_CLMcom-ETH-COSMO-crCLIM-v1-1 ()	4.7 (1.5 ... 20)	-0.67 (-1.3 ... -0.16)	2.1 (1.6 ... 2.7)	-0.53 (-0.77 ... -0.30)
MPI-ESM-LR_r1_GERICS-REMO2015 ()	1.7 (0.26 ... 14)	-0.29 (-1.3 ... 0.61)	1.5 (0.97 ... 2.1)	-0.29 (-0.56 ... 0.019)
NorESM1-M_r1_CLMcom-ETH-COSMO-crCLIM-v1-1 ()	0.52 (0.12 ... 2.1)	0.40 (-0.47 ... 1.2)	1.3 (0.91 ... 1.8)	-0.21 (-0.46 ... 0.064)
NorESM1-M_r1_GERICS-REMO2015 ()	0.66 (0.079 ... 9.2)	0.28 (-1.2 ... 1.6)	1.4 (0.87 ... 2.2)	-0.28 (-0.67 ... 0.099)

6 Hazard synthesis

We evaluate the influence of anthropogenic climate change on the events defined above by calculating the probability ratio as well as the change in intensity using observations and climate models. The observational datasets used to evaluate the 36-month SPEI over the Tigris-Euphrates Basin and Iran were ERA5 (both using the Hargreaves method to calculate PET and using direct PET model output) and SPEI as provided by the Global SPEI database. Models which do not pass the evaluation tests described above are excluded from the analysis. The aim is to synthesise results from models that pass the evaluation along with the observations-based products, to give an overarching attribution statement.

Figures 7 & 8 show the changes in probability and intensity for the observations (blue) and models (red). To combine them into a synthesised assessment, first, a representation error is added (in quadrature) to the observations, to account for the difference between observations-based datasets that cannot be explained by natural variability. This is shown in these figures as white boxes around the light blue bars. The dark blue bar shows the average over the observation-based products. Next, a term to account for intermodel spread is added (in quadrature) to the natural variability of the models. This is shown in the figures as white boxes around the light red bars. The dark red bar shows the model average, consisting of a weighted mean using the (uncorrelated) uncertainties due to natural variability plus the term representing intermodel spread (i.e., the inverse square of the white bars). Observation-based products and models are combined into a single result in two ways. Firstly, we neglect common model uncertainties beyond the intermodel spread that is depicted by the model average, and compute the weighted average of models (dark red bar) and observations (dark blue bar): this is indicated by the magenta bar. As, due to common model uncertainties, model uncertainty can be larger than the intermodel spread, secondly, we also show the more conservative estimate of an unweighted, direct average of observations (dark red bar) and models (dark blue bar) contributing 50% each. This is indicated by the white box around the magenta bar in the synthesis figures.

For both regions the intensity change estimates of observational and model assessments show a large overlap, and also the PRs for the Tigris-Euphrates show a considerable overlap. Therefore we report the weighted averages. For the PRs for Iran there is still overlap between models and observations, but

slightly less. For consistency we also report the weighted average for PR for Iran.

For the Tigris-Euphrates basin the PR is 25.2 (0.501 to 1420) for the weighted synthesis which corresponds to a change in intensity of -1.65 (-2.68 to -0.653). For Iran the weighted PR is 15.9 (0.779 to 371) corresponding to an intensity change of -1.63 (-2.44 to -0.828).

The intensity changes for the Tigris-Euphrates basin and Iran are statistically significant. Although the PRs for the Tigris-Euphrates basin and Iran encompass one, the best estimates are strongly positive while the upper bounds are very high. Combining this with the change in intensity, we decide to report the rounded best estimates as the main results: with PRs of 25 for TE and 16 for Iran. We also use the best estimates of the intensity changes to calculate the SPEI values we report as our overarching results. In 2023 the respective values of SPEI are -1.94 for TE and -1.82 for Iran, both corresponding to extreme drought (D3). In a 1.2C cooler climate the SPEI for TE would have been -0.29 and for Iran -0.19, corresponding to normal (non-drought) conditions with respect to the 1981-2010 climatology.

To understand the drivers behind this change we repeat the same analysis but for precipitation and temperature (see Fig.A3-A6)). For both regions we find that the changes identified in SPEI are primarily driven by the change in temperature which has an infinite probability ratio over both basins in both the weighted and unweighted synthesis. Over the Tigris-Euphrates basin this corresponds to a change in intensity of 2.04 (1.66 to 2.4) °C and of 2.56 (2.03 to 2.75)°C for Iran. It is important to highlight that the models represent temperatures over the river basin well, but less so over Iran with much more varied topography, hence confidence is high for the assessment over the Tigris-Euphrates basin, but medium over Iran.
In contrast to these strong trends in temperature the changes in precipitation are not significant with a PR of 1.44 (0.392 to 5.93) over the TE basin and 1.31 (0.322 to 5.51).

These results are corroborated when looking at the same event definitions but instead of in a 1.2°C cooler climate, in a 0.8°C warmer climate (Figs.9 & 10), although the projected changes are much smaller compared with the changes up to now, which is a well known problem with projecting extreme heat (van Oldenborgh et al., 2022). In particular, there is a projected further change in intensity of -0.68 (-1.61 to 0.25) for Iran and -0.82 (-2.62 to 1) for the Tigris-Euphrates basin which means a future SPEI value of -2.5 for Iran and -2.76 for the Tigris-Euphrates basin. In other words what is an extreme drought today (D3) would be an exceptional drought (D4) in a 2°C future.

Combining lines of evidence from the synthesis results of the past climate, results from future projections and physical knowledge we communicate that because of human-induced climate change drought severity has increased so much, that what is today classified as an extreme drought, would not have been classified a drought at all in a 1.2°C cooler climate. This is primarily driven by the very strong increase in temperature and thus PET.

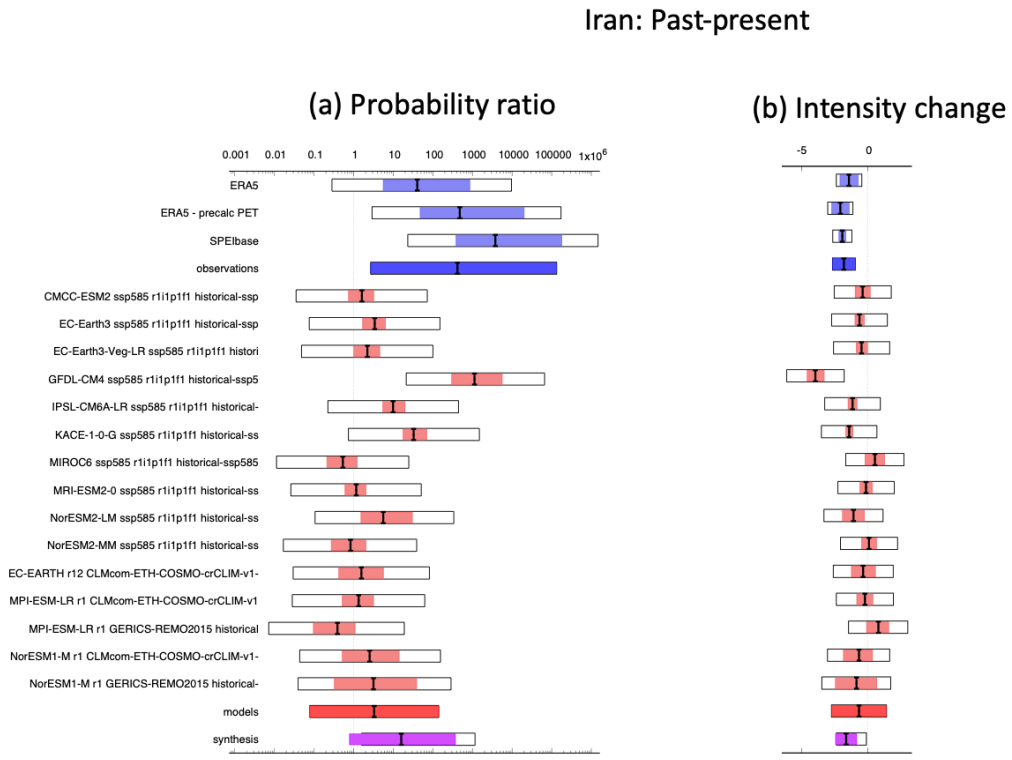

Figure 7: *Synthesis of (a) probability ratios and (b) intensity changes when comparing the return period and magnitudes of the 2020-2023 drought over Iran in the current climate and a 1.2°C cooler climate.*

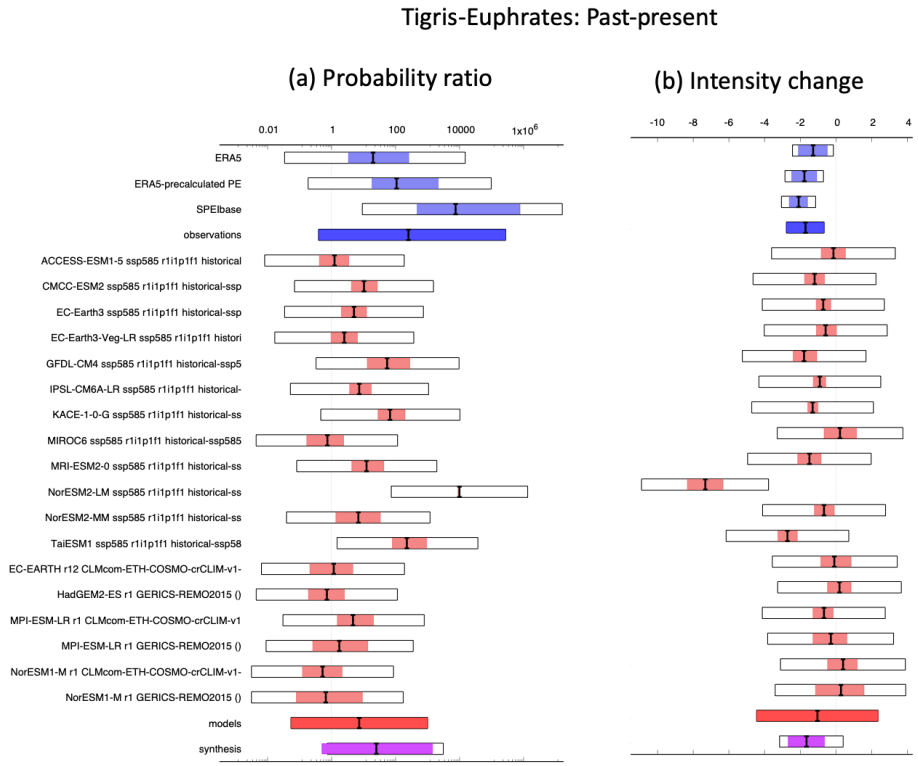

Figure 8: *Same as 7, over the Tigris-Euphrates river basin*

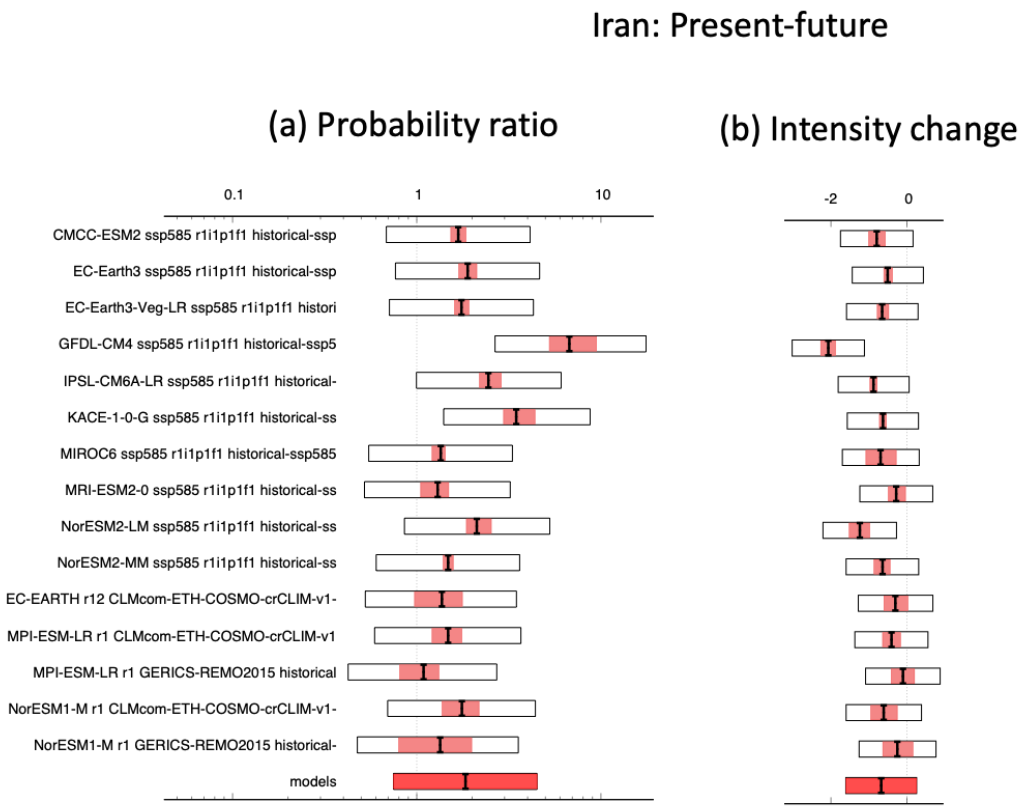

Figure 9: *Synthesis of (a) probability ratios and (b) intensity changes when comparing the return period and magnitudes of the 2020-2023 drought over Iran in the current climate and a future 2°C warmer climate.*

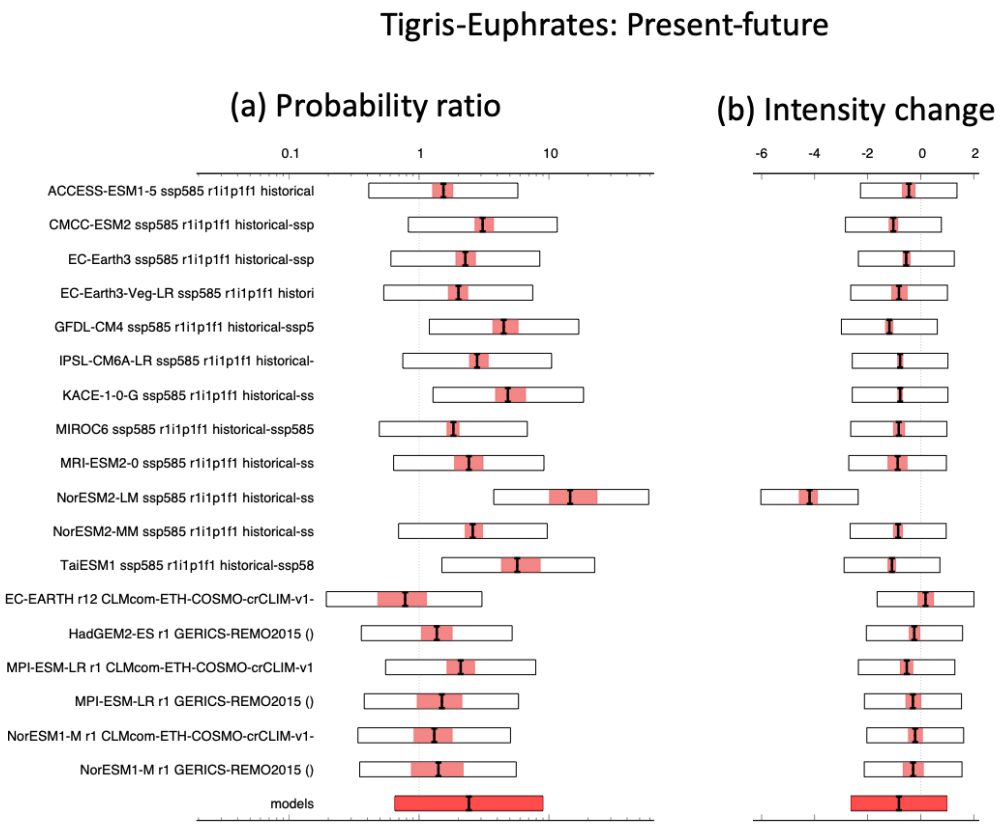

Figure 10: *Same as 9, over the Tigris-Euphrates river basin*

7 Vulnerability and exposure (V&E)

Since 1998, the MENA region has been subject to almost continuous meteorological, agricultural, and hydrological drought with varying impacts across countries (Muddathir, 2022). Across Iran, Iraq, and Syria, a combination of exceptionally low levels of rainfall, rising temperatures, water management practices, and vulnerability and exposure factors have resulted in a complex crisis with intersecting challenges primarily characterised by distinct factors of instability, fragility, and conflict in Iran, Iraq, and Syria resectivey. In these countries, widespread displacement, and loss of access to water, food, and electricity compound vulnerability to the impacts of drought. In the following section, we examine key themes of vulnerability, exposure, and adaptive capacity that contributed to or alleviated the impacts of the drought.

7.1 Conflict and fragility

In the Middle East and North Africa (MENA) climate change is a 'threat multiplier' mediating a number of potential security impacts as well as exacerbating fragility in countries already exposed to varying degrees of violence, conflict, regional-international governance challenges, and post-conflict transition (Water Peace and Security, 2021). The impacts of the ongoing drought threaten to roll back the region's development gains from the context of fragility in Syria and Iraq (once the world's fourth most fragile state) to Iran where fragility rankings have steadily improved since 2016. Despite varying levels of conflict and fragility Iran, Iraq, and Syria are simultaneously faced with drought-induced

limitations in nutrition and access to food, increases in the risk of wildfires and their attendant air quality challenges, as well as the rise and spread of water-related conflict, protests, internal displacement and migration (United Nations, 2021). Together these climate-conflict dynamics have created a complex crisis which may continue well into the future when climate, development, and security experts warn of destabilisation as the region is at risk to be the first to run out of water (Al-Delaimy, 2020). In this context, persistent rainfall decline punctuated by severe drought and water-related challenges not only present migration, livelihood and income concerns at the population level but also implications for the movement of armed groups, intercommunal conflict, and various forms of violence. This is especially true for urban areas where urbanisation rates are above average (over 65 percent) and 92 percent of the population live on 3 percent of the region's territory (GFDRR, 2019; FES, 2020).

The United Nations reports that people and countries most vulnerable to climate change also tend to be those most vulnerable to terrorist recruitment and violence (United Nations, 2021). Of the 15 countries most vulnerable to climate change, eight host UN peacekeeping or special political missions (ibid, 2021). However, the reality on the ground is more nuanced with interlinking vulnerability and exposure pathways related to poverty, weak governance, and the proliferation of terrorist activities compounding the impacts of climate and extreme weather events. Under these conditions, experiences of climate and extreme weather events including drought should be approached as one of several factors potentially driving anti-social outcomes such as recruitment into terrorist groups as well as negative coping mechanisms in the face of reduced adaptation choices. The link between drought and the rise of various forms of conflict and violence is therefore not a straightforward attribution (Selby et al, 2017). For example, in Iraq and Syria the Islamic State in Iraq and the Levant (ISIL) has allegedly exploited water shortages in its recruitment (IOM, 2022). However, this explanation under represents the contributing role of deep societal fractures including unmitigated urbanisation, social, economic, and ideological issues such as limited participation of those most impacted by fragility e.g., women and girls, in the political sphere (UNICEF, 2021).

A 2009 report by The International Institute for Sustainable Development (IISD) highlights the most important factors which can be considered in the drought-conflict nexus impacting the MENA region. These are increased competition for scarce resources; increased food insecurity; decreased economic growth; increased flows of migration and patterns of displacement; scarcity-induced militarization of key natural resources; and global inaction which can affect international and multilateral relationships (IISD, 2009). In Iran, systemic challenges and limited technical capacity exacerbated vulnerability. For example, the drought has reduced water supply for several decades at the same time as economic sanctions, water demand, irrigation practices, and inefficient use of water supply combine to mediate the dynamics of intercommunal tension and violence (von Hein, 2021). However in Syria, rapid urbanisation, chronic underemployment, and strictures in agriculture-based incomes exemplifies the mediating influence of climate-migration-and displacement in conflict affected countries in particular (Earth Day, 2020). Here, drought-related intensification of food insecurity threatens to worsen the complex crises of migration and displacement and extremism, in a region already facing political and religious splintering (ibid, 2020). Finally, in Iraq the concept of 'hydro-hegemony' finds full expression as water scarcity, the socio-political weaponization of water resources and dam practices, as well as increased tensions between states and states and non-state actors demonstrate the critical role which drought and water scarcity can play in cascading risks to stability, peace, and security across the region (King and Lehanne, 2021).

Ultimately, the dynamics of drought and conflict have a marked impact on the response capacity of humanitarian and development actors. For example, in September 2021, the UN's proposed response for mitigating the Syrian water crisis was estimated at US$200 million. However, this figure will barely assist the population of over 5 million people affected by the water crisis in the North of the country with estimates suggesting it will only reach 3.4 million people (Humanitarian Response, 2022). In Iraq, the 2021 – 2022 Disaster Response Emergency Fund (DREF) mobilised US$750,000 to support a little under 6,000 households (IFRC, 2023). While the operation signifies the potential for coordinated response, it also underpins the scale of the drought-related crisis as the humanitarian needs far outweigh the available resources (ibid, 2023). Humanitarian action alone is unlikely to solve the conflict-climate challenges in the region. This vital consideration prompts the need for prioritising climate action, awareness, and public participation in the region's governance agenda alongside key geopolitical challenges which have been shown to work together in tandem to exacerbate a fast growing and compounding crisis across humanitarian and development outcomes.

7.2 Environmental degradation and land-use changes

The Middle East, primarily arid or semi-arid, confronts escalating land degradation worsened by strongly increasing heat extremes linked to climate change (Lelieveld et al., 2016). IPCC projections foresee temperature spikes of 2°C within 15-20 years and over 4°C by the century's end, coupled with decreased precipitation (Majdi et al., 2022). Insufficient rainfall leads to dry soil, leading to more dust storms, which can alter cloud properties and reduce precipitation in polluted areas (Rosenfeld et al., 2001). In arid regions, evaporation rates surpass precipitation and natural recharge rates, causing natural salinization of groundwater (UNEP, 2007).

The rain deficit in the region is leading to a web of other interconnected issues in the three countries. Desertification is one of the significant issues faced by all three countries. Desertification is known to cause problems such as reduced land productivity leading to reduced vegetation cover, loss of biodiversity, and increased frequency of dust storms, to name a few (Carvalho, 2022; McSweeney, 2019).

Iraq, burdened by war aftermath, rapid urbanisation, and poor planning, faces water scarcity, air pollution, and biodiversity loss (World Bank, 2017). Unilateral dam projects upstream of the Tigris and Euphrates have resulted in a significant reduction in the quantity and quality of water in Iraq (Mahdi & Fawzi, 2014). This reduced water level has led to rising salt levels and deteriorating water quality. Due to annual evaporation rate reaching up to 3 metres and reduced river water levels, seawater has encroached inland to al-Qurnah, a town located on the joining point of the Tigris and Euphrates rivers, resulting in the devastation of 60,000 acres of farmland and loss of around 30,000 trees (United Nations, 2022). Low rainfall, unsustainable agrarian practices, and diminishing vegetation cover due to conflict, soil erosion, and contamination have intensified water shortages and desertification in Iraq (United Nations, 2022). Additionally, more than 20,000 km² of marshes, equivalent to 90% of their total area, were dried, significantly impacting the region. These marshes, once rich in plant, agricultural, animal, and fish resources, played a crucial role in preserving environmental balance. Recent studies indicate a high risk of land salinity and an inevitable loss of animal settlement areas due to the drying of these marshes (Fartm, 2020;Larsen, 2011).

Iran has witnessed rapid deforestation over the past fifty years, driven by intense cultivation and mismanagement, resulting in environmental problems and soil degradation (Hosseini & Ashraf, 2015). Land use changes have disrupted soils that once thrived under natural forests in northern Iran,

as documented in studies (Bahrami et al., 2010). Iran, where Ramsar Convention was signed in 1971, has 25 wetlands registered in the convention (Middle East Monitor, 2022). The country is facing a significant challenge to protect and preserve its wetlands. It has been reported that out of 25 wetlands registered under the Ramsar convention, one-third are on the brink of drying out. However because of factors such as drought, mismanagement such as illegal redirecting of water for agricultural purposes (Mehrnami, 2023), and reduced water inflows into marshes, many Iranian wetlands have experienced degradation in recent years. This degradation has led to diminished biodiversity and ecological functions, resulting in socio-economic damage for the country (Department of Environment, 2011)

The Syrian war, which began in March 2011, has resulted in the displacement of over half of the Syrian population. Those internally displaced have been compelled to leave their homes, seeking safety, particularly in the Syrian coastal region (SCR). Syria's vegetation, a vital natural resource, is predominantly concentrated in the humid coastal area, accounting for more than 90% of the total vegetation (Barakat et al., 2014). A study conducted in the Safita area of Tartous, Syria, revealed significant variations in vegetation cover. Degradation has primarily affected areas with high and very high vegetation densities in the humid coastal regions. This degradation is attributed to factors such as fuel shortages, population growth, and intentional fires, leading to soil erosion and an increased risk of degradation (Abdo, 2018). Additionally, land degradation in Syria is caused by wind erosion especially in the Syrian Badia, excessive grazing that destroys natural vegetation, land pollution, uncontrolled urban development, and rising soil salinity (Land Degradation Neutrality target Setting Programme, 2020)

All three countries are dealing with significant land degradation due to various issues such as lack of rainfall, poor water management, and rapid urbanisation. These issues have resulted in salinity problems, reduced arable land, and loss of vegetation cover, which in turn is leading to desertification. It is crucial to address these problems to protect the natural environment and ensure the countries' ecological and economic sustainability as the climatological and systemic factors driving these conditions are expected to persist in the future.

7.3 Water and drought risk management

7.3.1 A multifaceted water crisis

In recent decades, Iraq, Syria, and Iran have experienced more intense and frequent droughts (Nazari et al., 2018; Mohammed & Fallah, 2019; Hameed et al., 2018). Beyond this drying trend, confirmed by this study, the high levels of water stress in the region today is also driven by rapid population growth, industrialization, land-use changes, environmental degradation, aged water treatment plants, and low efficiency of irrigation water systems (Nazari et al., 2018, Saatsaz, 2019; Mason, 2022; Madani, 2014). On average across the region, agricultural practices currently consume 80% of freshwater resources, mainly through irrigation (ACSAD & ESCWA, 2021). As laid out in section 7.1, water is moreover weaponized and used as an instrument of power in conflict, with water systems increasingly targeted for sabotage and capture by armed forces to control distribution of water (Gleick, 2019; Abbara et al., 2021). For example, the Islamic State has been known to seize Iraqi and Syrian dams to intentionally flood locations, poison water sources, and restrict hydroelectricity generation in locations over which they endeavoured to bolster their control (von Lossow, 2016).

Most notably, transboundary water management and associated politics constitute key factors to water security in the region, since over a dozen international rivers flow through the three countries of focus (Al-Faraj et al., 2015; Al-Ansari, Ali, & Knutsson, 2014; UNESCO, 2016). Treaties on shared usage of water from Euphrates, Tigris, and Orontes are in place between Syria, Iraq, Türkiye, Lebanon, and Jordan, including minimum water quotas during scarce times, but limited and underdeveloped monitoring systems and a weak compliance mechanism renders Syria particularly disadvantaged during droughts (UNESCO, 2016). Located furthest downstream, Iraq, heavily reliant on the Tigris and Euphrates, is also notably vulnerable to Türkiye and Iran's water resource management, as they control the headwaters of most rivers that run through Iraq (Al-Faraj et al., 2015).

In Iraq, measures deployed to address water scarcity include improving water treatment plants, rehabilitating water infrastructure including water pumps and pump stations, water conservation projects and campaigns, and increasing farmers' access to irrigation wells (McLinden, 2022). In Syria, water pumping stations have been rehabilitated and wastewater treatment plants installed, with increasing wetland conservation and protection (ICRC, 2021; UNICEF, n.d.; Asswad, 2021). Unless root causes are adequately addressed, however, water scarcity in the region will pose a further escalating threat to drinking water and food security, and is estimated to increase poverty among rural communities and drive forced migration (Nazari et al., 2018). As a result, it could contribute to aggravated conflict and intercommunal violence over limited water resources (Nazari et al., 2018).

7.3.2 The policy landscape

According to UNESCO (2016), drought management policies in Syria have historically focused on mitigating exposure to drought and treating the symptoms of drought. In doing that, it promoted maladaptation to drought risk, stemming from a lack of awareness of rapidly increasing variability in water supply in the 1970s. Examples include subsidising unsustainable livestock management and wheat cultivation. This changed when Syria's National Drought Strategy was developed by the Ministry of Agriculture in 2005, and finally approved in 2009, as it now focused on addressing underlying vulnerabilities, keeping socioeconomic impacts at a minimum, and facilitating recovery post drought (UNESCO, 2016). Over the following years, a National Drought Steering Committee, National Drought Task Force, and National Fund for Drought Mitigation were established to prepare and review drought risk management plans, oversee proposals on reducing household vulnerability, and promote financial sustainability for implementation of the agricultural sector's drought policy.

In Iraq, while the country is still lacking a national water law, the current water management policy, the Strategy for Water and Land Resources in Iraq (SWLRI), was adopted in 2014 and outlines the core principles for water governance until 2035 (Water, Peace, and Security, 2022). A study by Al-Faraj et al. (2015) suggests that the policy is inherently flawed owing primarily to its focus on emergency response and lack of consideration to risk management, with barriers to effective drought risk management strategies including limited knowledge on preemptive drought management and planning, a lack of technical capacity, a deficit of reliable data on historical drought impacts on various sectors, and protracted conflict having weakened and delayed stakeholder engagement (Al-Faraj et al., 2015). Von Lossow (2022) further underscores that decentralisation, with fragmented responsibilities, coordination and action, compromises local water management and national water security, along with an unfulfilled water allocation framework that does not effectively address the underlying causes of the water crisis to begin with.

Following the increase in the number of and impacts from droughts throughout the past decades, Iran has enacted a set of laws to manage the threat (Moghaddam & Faryadi, 2021). However, lacking a legal mechanism to support prevention, mitigation, adaptation, institutionalisation, empowerment, and compensation leaves Iran's current body of laws unfit for purpose. Moghaddam and Faryadi (2021), suggests that the country needs a comprehensive law on the management of drought, along with its integration into development plans. Further, Neisi et al. (2020) highlight the need to center farmers in policy-making, empowering them to make their own risk management decisions with a wide range of tools and strategies available.

7.3.3 Household coping strategies

Given the compounding nature of the ongoing crisis in the region, driven not only by drought but a range of factors, notably conflict, this subsection will include coping mechanisms which are deployed to address the cumulative stress that burdens households.

In Iran, attitudes, personal norms, objective barriers, and subjective barriers are known to influence whether and which of the coping activities are deployed by farmers - one of the most severely impacted groups by drought (Khoshnodifar et al., 2023). Non-erosive activities center around the management of farms, crops, finances, irrigation and water, and physical infrastructure, and social activities, and include crop diversification, multi-crop agriculture, and migration (Khoshnodifar et al., 2023; Savari and Moradi, 2022; Ashraf and Kumar, 2013). These are common in Syria and Iraq as well (see e.g. Dinc & Eklund, 2023; WPS, 2023). However, over time, households across the three countries have increasingly resorted to erosive coping strategies which sacrifice long-term resilience by creating further vulnerability to food insecurity and aid dependence (CARE, 2022). In Syria, parents are left to choose between paying for urgent medical treatments or feeding the family, and buying firewood for heating the home or sending children to school (CARE, 2022). It is common for households to eliminate nutritious but expensive foods such as fruits, vegetables, and meat; sell off farmland; and pull children out of education to send them to work. In 2022, CARE reported that over half of the children in Syria had been deprived of education, and that over 40% of daughters had been married off before turning 18 years. In Iraq, one-third of households have sold off their property to buy food, and three-quarters have bought food on credit or by borrowing money (NRC, 2021). Further, families have reported reducing both the number and sizes of meals (IFRC, 2021). According to IOM (2023), drought has displaced 62,000 people across Southern Iraq, and led to the full abandonment of ten locations, most of which are located in Thi-Qar Governorate. Ensuing inability to engage in income-generating activities exacerbates the pre-existing vulnerabilities faced by these displaced communities, and often contributes to additional erosive coping strategies (NRC, 2021).

7.3.4 Drought response

In August 2021, the IFRC's Disaster Relief Emergency Fund (DREF) mechanism was activated for the drought in Iran, targeting over 83,000 people (IFRC, 2022a). The operation was subsequently extended in March 2022. By August 2023, the Iranian Red Crescent Society (IRCS) had assisted more than 54,000 people by interventions which include distribution of food, dignity kits, masks, first aid kits, medicine, and health and hygiene promotion activities (IFRC, 2022a).

In Iraq, a DREF operation was activated between September 2021 and August 2022, and enabled the Iraqi Red Crescent Society (IRCS) to target over 43,000 affected people (IFRC, 2023a). Three mobile health clinics were mobilised to provide primary health care and psychosocial support, four water

treatment and desalination points were installed, and two emergency response units remained on standby to provide services such as water treatment, storage, and distribution, as well as hygiene promotion (IFRC, 2023a). Additionally, IRCS distributed one-time cash assistance of $100 and food parcels to support families in meeting their most urgent needs. In 2022, FAO activated the Special Fund for Emergency and Rehabilitation Activities (SFERA-AA) in response to drought, targeting Erbil, specifically Diwaniyah, Kirkuk, Kurdistan, and Najaf (FAO, 2022). Actions included distribution of drought tolerant seeds and fertilizers as well as training on good practices. The target population included 1.130 households at risk.

Reaching the worst conditions in 70 years, the drought in Syria triggered the DREF between October 2021 and April 2022 (IFRC, 2022b). Staff and volunteers at local to national level throughout the Syrian Arab Red Crescent (SARC) monitors the drought and coordinates stakeholder engagement, response planning, and implementation, assisting roughly 15,000 people across the affected areas. SARC operates four health facilities, promotes community engagement and awareness-raising activities, and has rolled out 41 water system rehabilitation projects since 2020. Further, food and livelihood interventions have been distributed, including seeds and installations of water pumps (IFRC, 2022b). Similarly, in 2023, a DREF was launched targeting 650,000 people affected by drought in Al-Suweida in southern Syria (IFRC, 2023b). Interventions included rehabilitation of boreholes, maintenance of pumps, and installation of water tanks. SARC staff and volunteers conducted awareness raising among the affected population on clever use of water in households. FAO also launched a SFERA-AA activation, targeting 2,565 households across the Deir ez-Zor and Raqqa Governorates (FAO, 2021). Actions included distribution of drought-tolerant wheat seeds and training centered on climate-smart agriculture.

7.4. V&E Conclusions

The recent drought in Iran, Iraq, and Syria is a compelling lens through which to understand and assess the complex crisis facing vulnerable people and communities across the MENA region. It is also a harbinger of a reality and norm which could affect vulnerable groups across the globe as human-induced challenges spanning fragility, conflict, and climate change yield unprecedented impacts. Between record low levels of rainfall, rising temperatures, water management practices, and vulnerability and exposure factors spanning displacement and migration, collapse of key infrastructure and economic sectors, limitations in technical capacity, governance challenges, fragility, conflict,and violence; the problems seem intractable. Within this regional and domestic context, climate change has acted as a ‘threat multiplier’, mediating a number of potential security impacts as well as exacerbating fragility and constraining domestic, regional, and international efforts to respond to the resulting humanitarian crisis.

The climatological factors increasing exposure and vulnerability to the impacts of drought including rain deficit, dust storms, desertification, insufficient rainfall - which leads to dry soil and reduced precipitation in polluted areas - as well as salinization of groundwater compound the direct impacts of the drought. However, the contributing role of governance, water management, and technical capacity issues cannot be understated as high levels of water stress in the region are driven by rapid population growth, industrialization, unmitigated land-use changes, aged water treatment plants, and low efficiency of irrigation water systems. Vitally, as climatological and systemic failures mutually influence domestic and regional policy, relationships between states and state and non-state actors; water is increasingly weaponized in conflict, water systems are sabotaged, and transboundary water

management practices yield even greater outcomes of vulnerability at the population level. Although drought has encouraged countries across MENA to pay attention to the impacts of climate and extreme weather events through anticipatory action, law, and policy these interventions need to be flexible and proactive to a rapidly changing landscape of unprecedented extremes. To increase resilience in the future, comprehensive law and policy, adherence to international humanitarian law and customs on natural resources management, cooperation, and integration of local and indigenous knowledge, norms, and coping mechanisms should be equally prioritised in DRR and climate action.

As the drought and compounding impacts of conflict, displacement, post conflict transition, and fragility interact; interventions aimed at mitigating exposure and vulnerability to drought need to be seen in relation to the complex and fragile context in which they are implemented.

Appendix

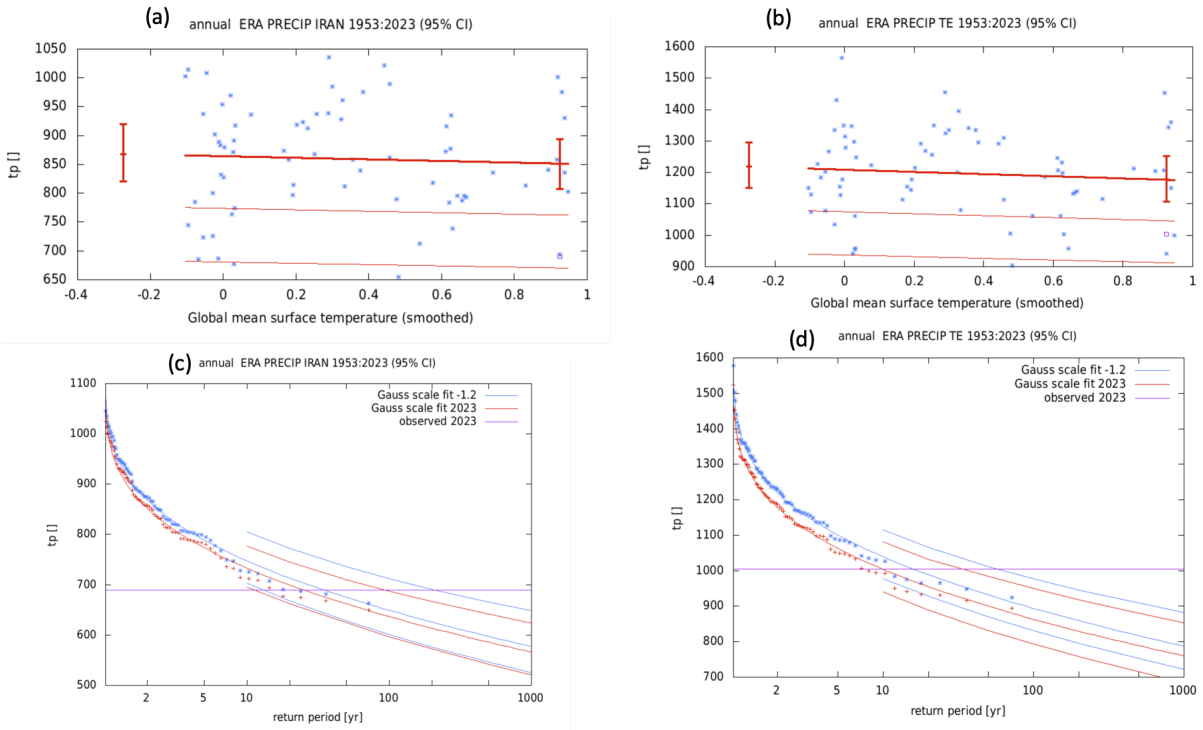

Figure A1 Top: Observed 36-month rainfall as a function of the smoothed GMST for (a) Iran and (b) Tigris-Euphrates basin.. The thick red line denotes the time-varying location parameter. The vertical red lines show the 95% confidence interval for the location parameter, for the current, 2023 climate and a 1.2ºC cooler climate. The 2023 observation is highlighted with the magenta box.
Bottom: Gaussian fit with constant dispersion parameter, and location parameter scaled proportional to observed GMST, for (c) Iran and (d) Tigris-Euphrates basin. The 2023 event is included in the fit. The magenta line shows the magnitude of the 2023 event analysed here.

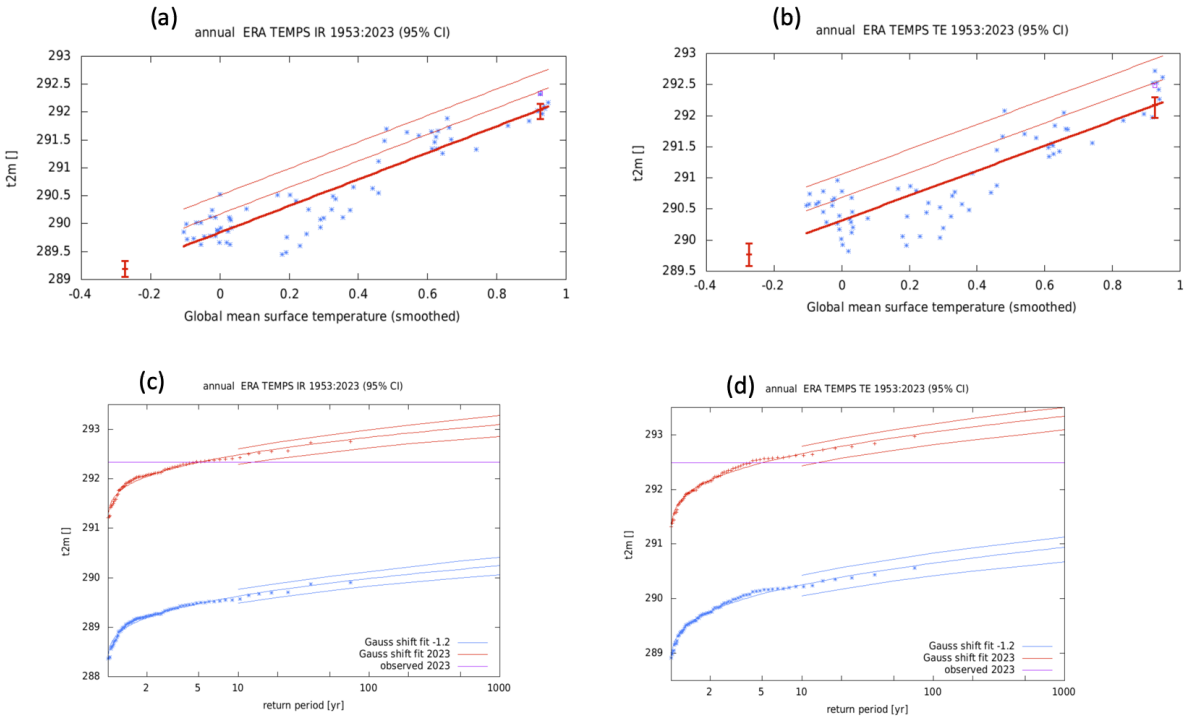

Figure A2 Top: Observed 36-month temperature as a function of the smoothed GMST for (a) Iran and (b) Tigris-Euphrates basin.. The thick red line denotes the time-varying location parameter. The vertical red lines show the 95% confidence interval for the location parameter, for the current, 2023 climate and a 1.2ºC cooler climate. The 2023 observation is highlighted with the magenta box.

Bottom: Gaussian fit with constant location parameter, shifted proportional to observed GMST, for (c) Iran and (d) Tigris-Euphrates basin. The 2023 event is included in the fit. The magenta line shows the magnitude of the 2023 event analysed here.

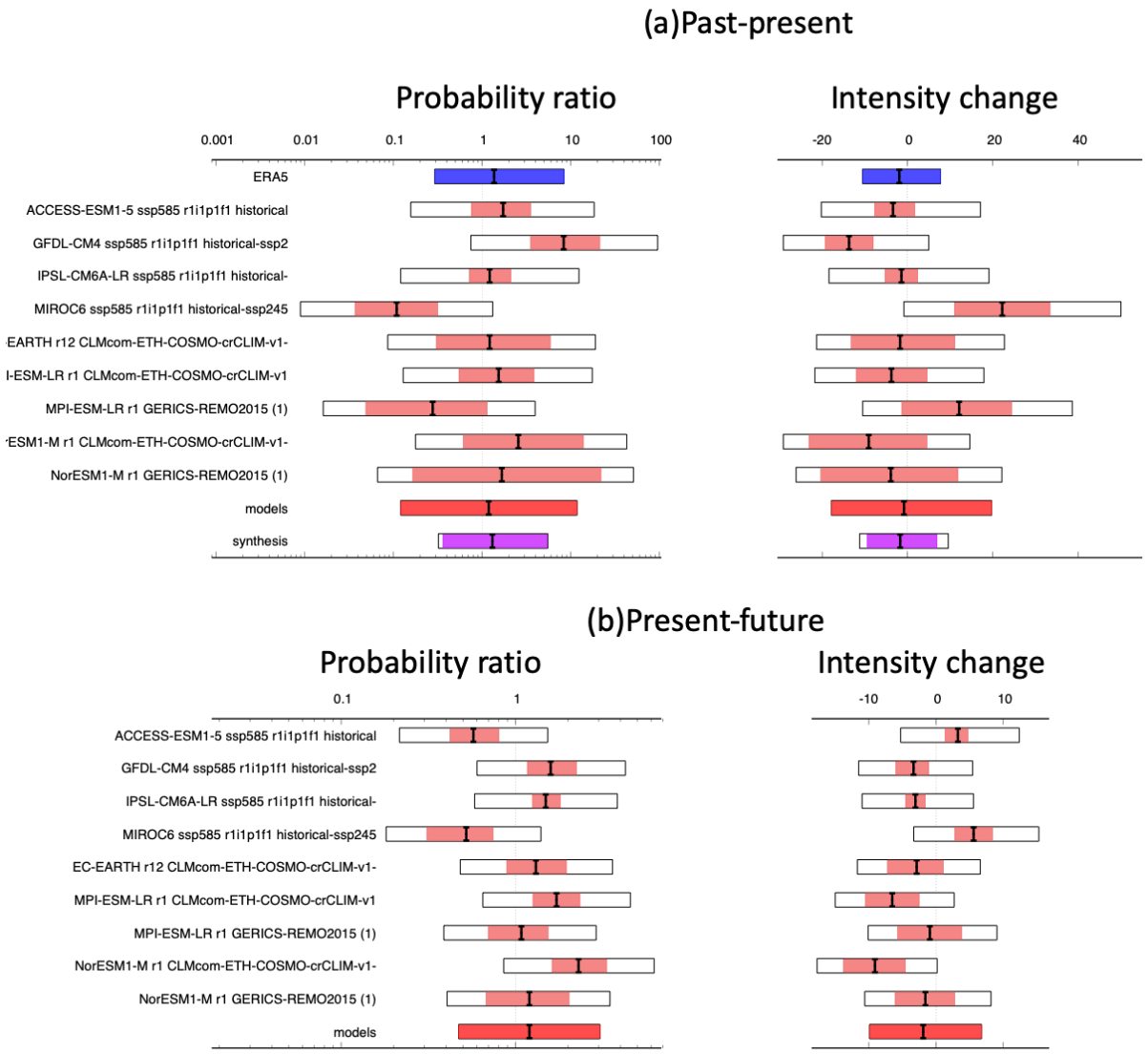

Figure A3: *Synthesis of probability ratios (left) and intensity changes (right) when comparing the return period and magnitudes of the 2020-2023 precipitation deficit over Iran in (a) the current climate and the past 1.2°C cooler climate and (b) same as (a) in the current climate and a future 2°C warmer climate*

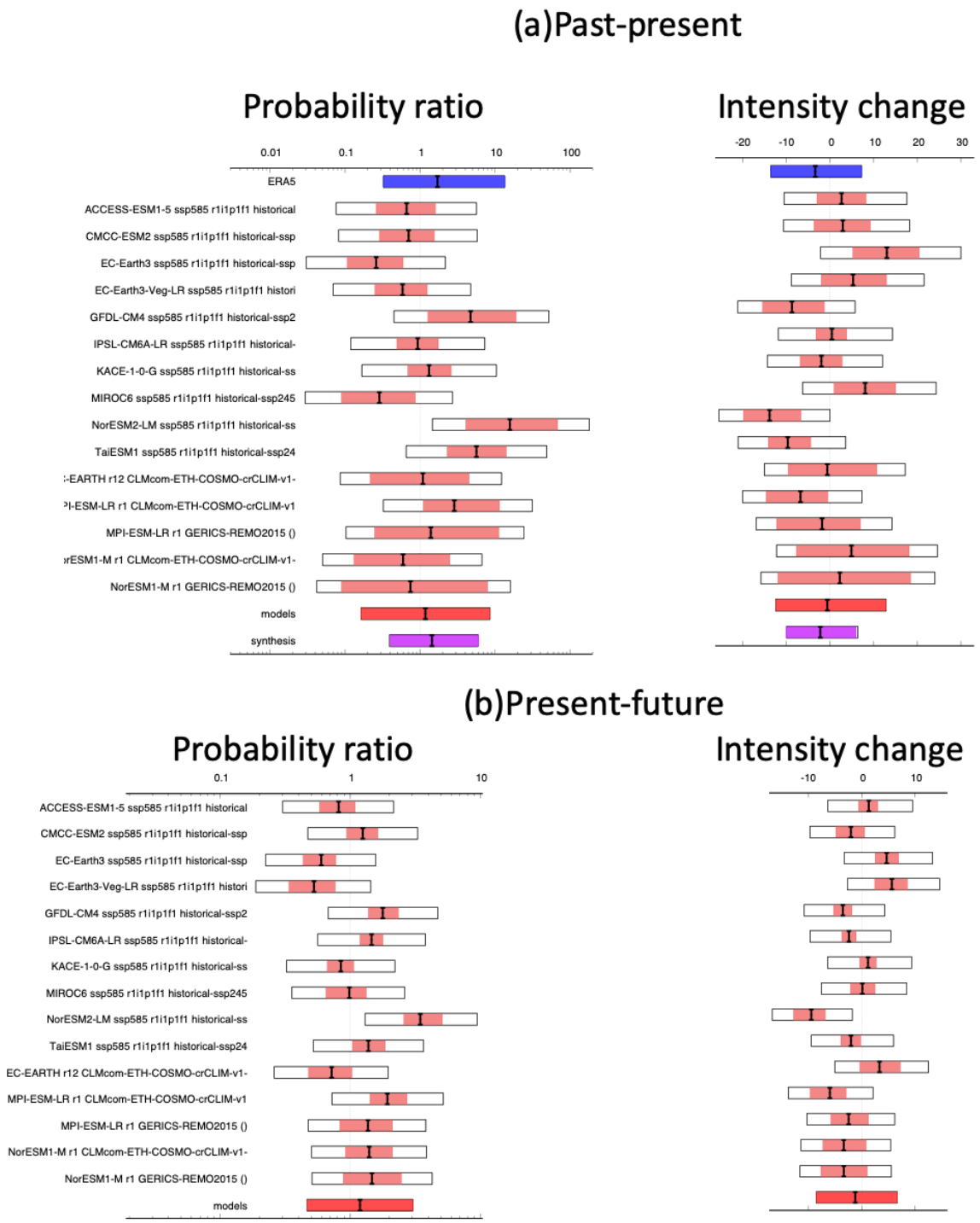

Figure A4: *Same as above for Tigris-Euphrates basin*

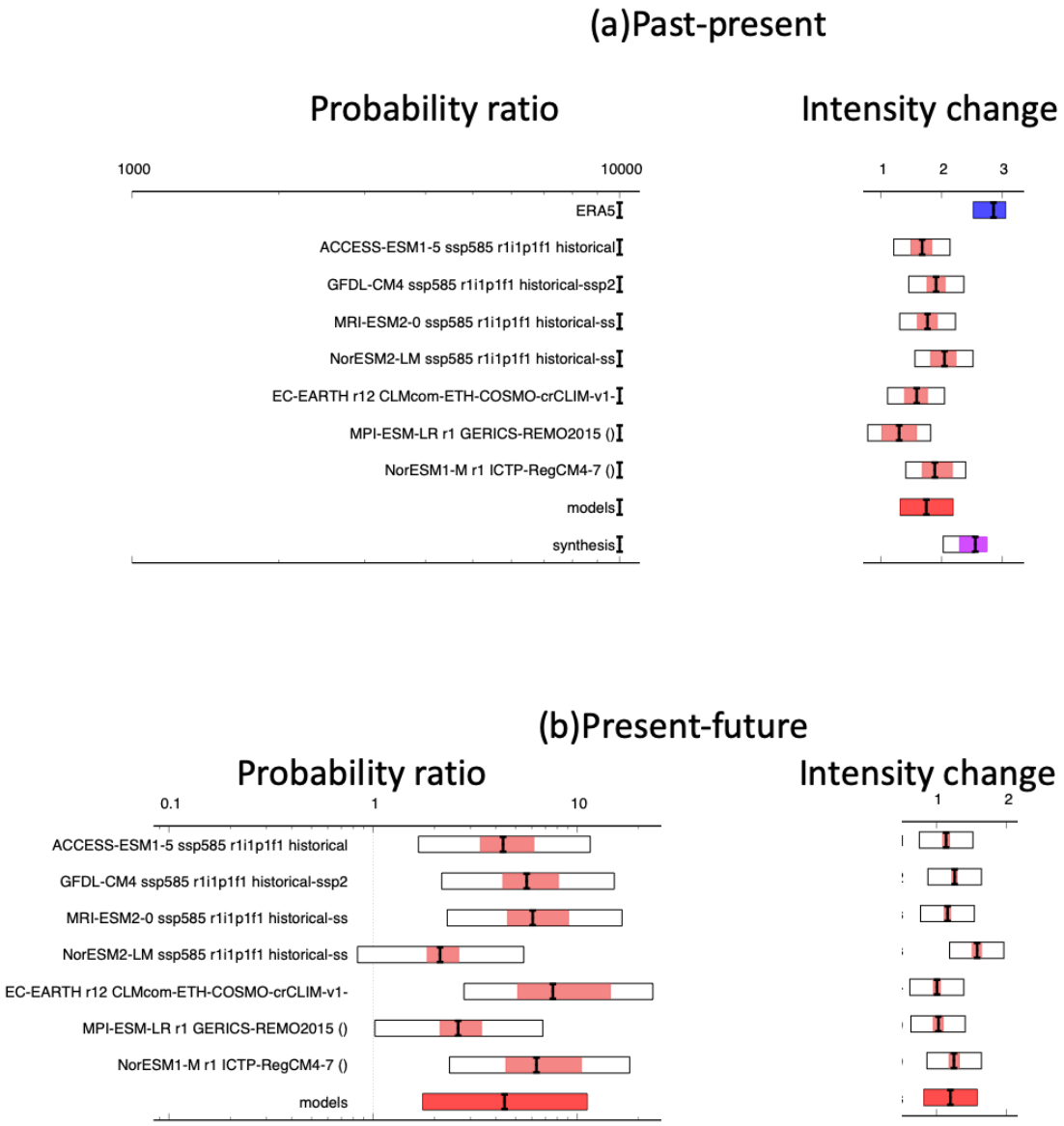

Figure A5: *Synthesis of probability ratios (left) and intensity changes (right) when comparing the return period and magnitudes of the 36 month average temperature from 2020-August to 2023-July over Iran in (a) the current climate and the past 1.2°C cooler climate and (b) same as (a) in the current climate and a future 2°C warmer climate*

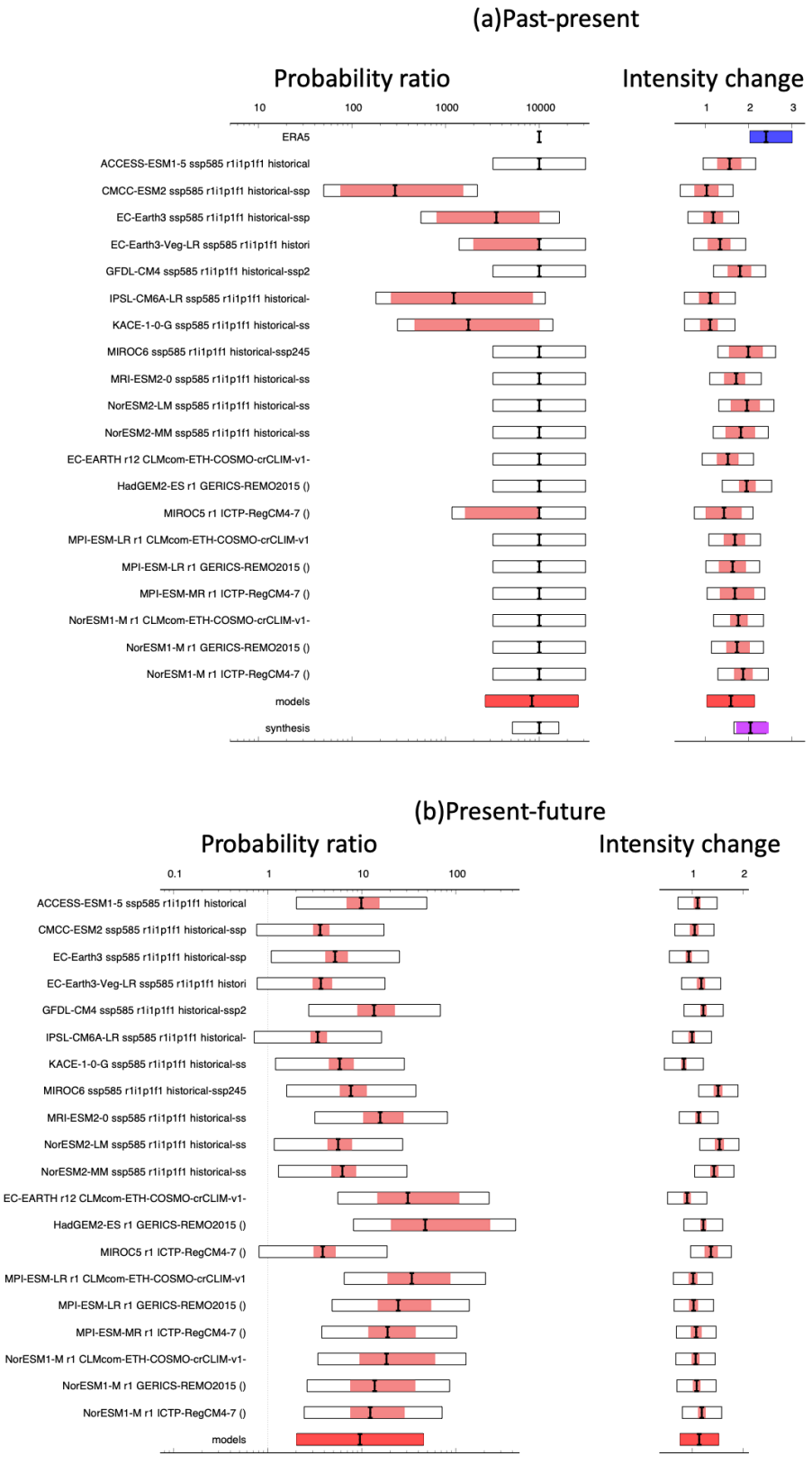

Figure A6: *Same as above for Tigris-Euphrates basin*

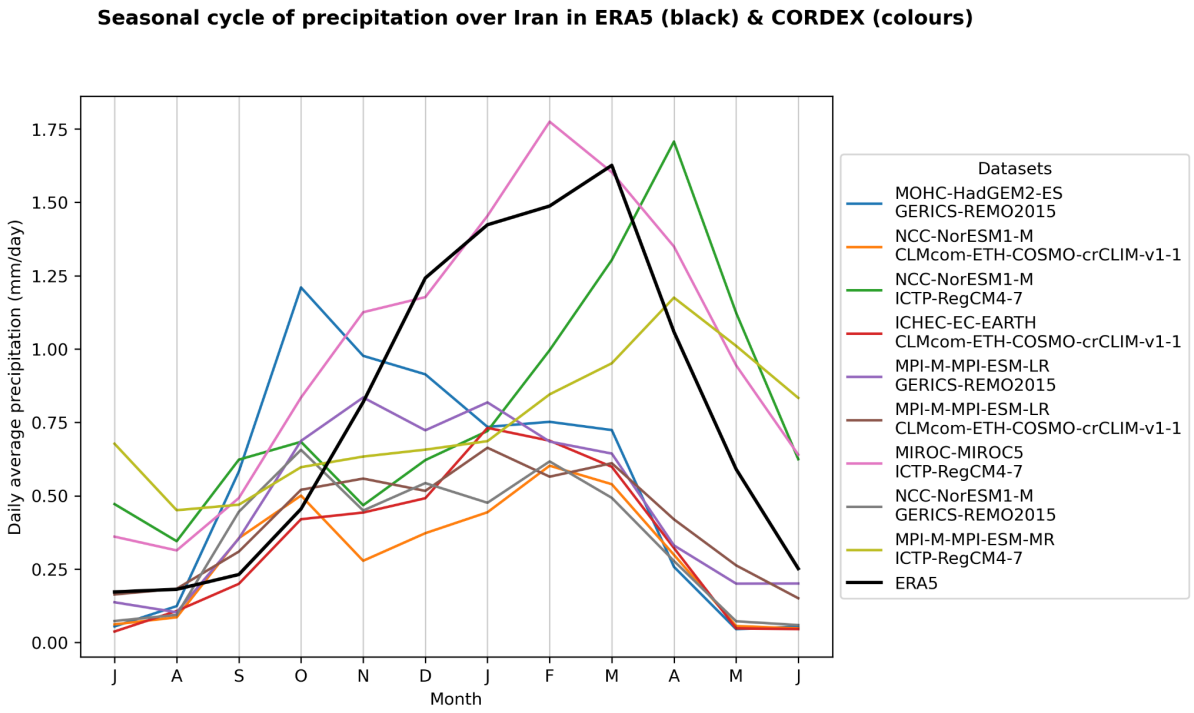

Figure A7: *Seasonal cycle of precipitation over Iran in ERA5 and different CORDEX models as used for model evaluation (sec. 4).*

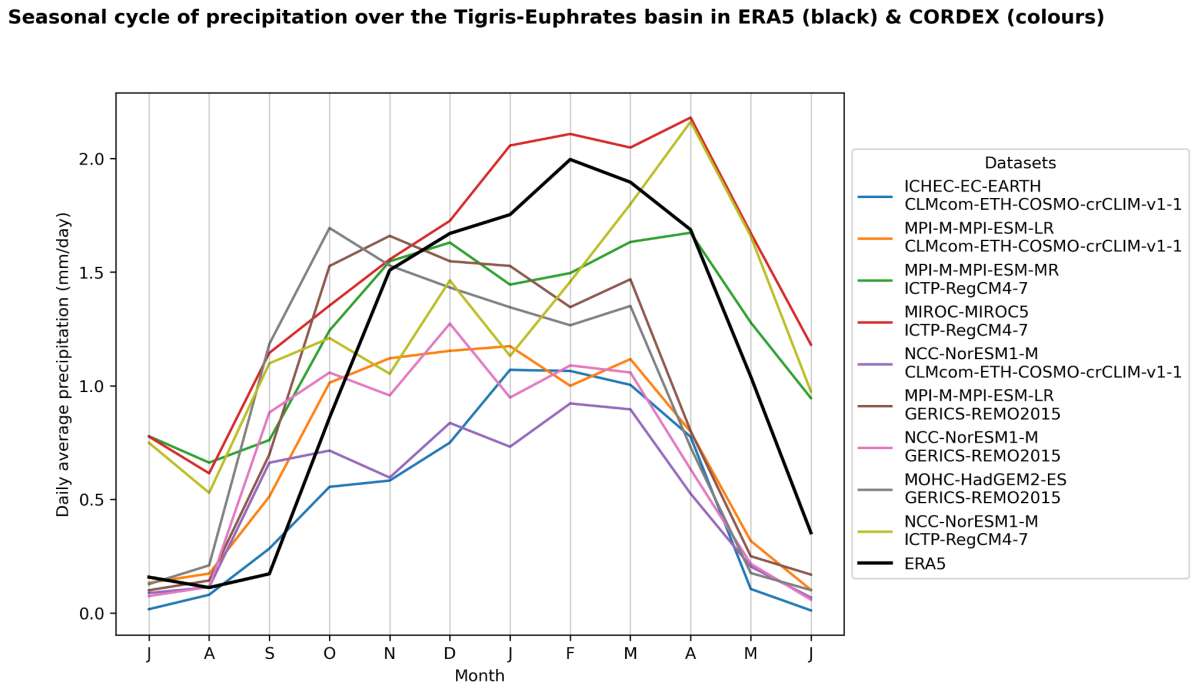

Figure A8: *As figure A8 but for the Tigris-Euphrates basin.*

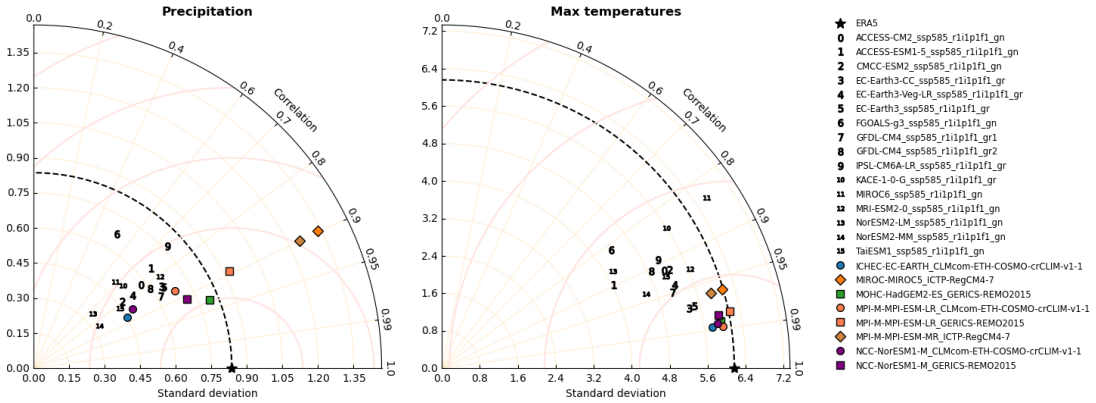

Figure A9: *Taylor diagrams showing the correlation of ERA5 with the amplitude of spatial patterns in CORDEX and CMIP6 models as used for model evaluation (sec. 4).*

Data availability

All data are available via the Climate Explorer.

References

All references are given as hyperlinks in the text.